보건학석사 학위논문

Degradation mechanisms of Iopromide during the UV-LEDs/chlorine reaction

UV-LEDs/chlorine 공정에서의 iopromide 분해 메커니즘 연구

2022 년 2 월

서울대학교 보건대학원
환경보건학과 환경보건학전공
차 영 호

Degradation mechanisms of Iopromide during the UV-LEDs/chlorine reaction

UV-LEDs/chlorine 공정에서의 iopromide 분해 메커니즘 연구

지도 교수 조 경 덕

이 논문을 보건학석사 학위논문으로 제출함
2021 년 12 월

서울대학교 보건대학원
환경보건학과 환경보건학전공
차 영 호

차영호의 보건학석사 학위논문을 인준함
2022 년 1 월

위 원 장	최경호	(인)
부위원장	이승묵	(인)
위 원	조경덕	(인)

Contents

List of Table

Abstract

Iopromide (IPM) is a representative iodinated contrast media compound for diagnostic medicine, and is widely detected in hospital wastewater due to its high consumption and biochemical stability. In this study, three different UV-LED wavelengths (265, 310, 365 nm) were used in the UV-LED/chlorine reaction to investigate the degradation mechanism of IPM. Although fluence-based rate constant (k'_{IPM}) was decreased with increasing wavelengths (6.55×10^{-2} cm^2 mJ^{-1} at 265 nm to 1.00×10^{-5} cm^2 mJ^{-1} at 365 nm), the synergistic effect of UV-LED and chlorine was greater at a higher wavelength (k_{obs} increased 99 times at 365 nm). At 265 nm, the degradation rate of IPM increased from pH 6 to 8. However, at 310 nm and 365 nm, the degradation rate of IPM was decreased as pH increased. Radical scavenging experiment showed that the contribution of OH• increased as wavelength increased (2.4% at 265 nm to 16.4% at 365 nm). On the other hand, the contribution of RCS decreased as wavelength increased (93.2% at 265 nm to 82.5% at 365 nm). The largest portion of RCS was found to be ClO• (70~80% among RCS). Among nine transformation products (TPs) during the UV-LED/chlorine reaction of IPM, TP-699, TP-667, and TP-607 were newly identified in this study, and TP-699, a chlorinated transformation product of IPM, was only detected with higher levels at lower wavelength. As a result of the Microtox inhibition test using *V. fischeri*, no increase in toxicity was observed in all three wavelengths. This study can provide information for selecting an appropriate wavelength when applying UV-LED to WWTPs through a radical contribution experiment.

Keywords: *Reactive chlorine species; hydroxyl radical; UV-LED; iopromide; transformation products (TPs); Microtox.*

Chapter 1. Introduction

1.1. Study Background

With the development of the public health and medical care system in recent decades, the discharge of pharmaceuticals and personal care products (PPCPs) to the water environment is rapidly increasing (Wu et al., 2015; Roberts et al., 2016). Among the various PPCPs, iodinated X-ray contrast media (ICM) is consumed by 3.5×10^6 kg per year worldwide, and is known to be metabolically stable and excreted quickly through urine or feces (Pérez and Barceló, 2007). ICM is a form of intravenous radiocontrast agent containing iodine, which enhances the visibility of vascular structures and organs during radiographic procedures (Bettmann, 2004). ICM generally constitutes more than 3% of all PPCPs discharged from wastewater (Giri and Pal, 2014).

Iopromide (IPM), known as a representative indicator compound of ICM (Zhang et al., 2021), was detected up to 10 μg/L at a river in South Korea in 2020, the highest level among 14 target PPCPs (Seo et al., 2020). Recently, the monitoring data of IPM from 20 wastewater treatment plants (WWTPs) at 10 countries showed that WWTPs cannot remove IPM effectively. Only two WWTPs showed a removal rate of over 90 % through secondary clarifier (Sengar and Vijayanandan, 2021). Moreover, if the ICM undergoes chemical treatment processes (i.e. chlorination), mutagenic and genotoxic transformation products (TPs) can be produced (Rastogi et al., 2014). In the case of IPM, the luminescence inhibition rate of *V. fischeri* increased to 100% after the UV photolysis process (Fabbri et al., 2016). However, among recent studies on PPCPs, research on ICM removal is lacking

(Zhang et al., 2021). Therefore, it is necessary to find the appropriate method to efficiently and safely remove IPM in water.

According to recent studies, advanced oxidation processes (AOP) such as UV/H_2O_2 or ozonation are inefficient for removing ICM, but low reactivity with OH• and O_3 Were reported (Kong et al., 2018; Zhang et al., 2021). Among the radicals, reactive chlorine species (RCS) can be the alternative option to degrade IPM in hospital wastewater. Therefore, UV/chlorine process can be the alternative option since various reactive chlorine species (RCS) (e.g., •Cl, •Cl_2^-, and •ClO) can be produced during the UV/chlorine reaction, as shown in Eqs. (1)-(7) (Zehavi and Rabani, 1972; Kläning and Wolff, 1985; Jennings et al., 2001; Matthew and Anastasio, 2006; Fang et al., 2014; Guo et al., 2017).

$$HOCl / OCl^- \xrightarrow{h\nu} OH\bullet / O\bullet^- + Cl\bullet \quad (1)$$

$$Cl\bullet + Cl^- \xrightarrow{k_1} Cl_2\bullet^- \quad (k_1 = 6.5 \times 10^9\ M^{-1}s^{-1}) \quad (2)$$

$$Cl_2\bullet^- \xrightarrow{k_2} Cl\bullet + Cl^- \quad (k_2 = 1.1 \times 10^5\ M^{-1}\,s^{-1}) \quad (3)$$

$$OH\bullet + HOCl \rightarrow ClO\bullet + H_2O \quad (k = 2.0 \times 10^9\ M^{-1}s^{-1}) \quad (4)$$

$$OH\bullet + OCl^- \rightarrow ClO\bullet + OH^- \quad (k = 8.8 \times 10^9\ M^{-1}\,s^{-1}) \quad (5)$$

$$Cl\bullet + HOCl \rightarrow ClO\bullet + H^+ + Cl^- \quad (k = 3.0 \times 10^9\ M^{-1}\,s^{-1}) \quad (6)$$

$$Cl\bullet + OCl^- \rightarrow ClO\bullet + Cl^- \quad (k = 8.2 \times 10^9\ M^{-1}\,s^{-1}) \quad (7)$$

While OH• is a non-selective oxidative radical (Watts and Linden, 2007), other radicals such as Cl•, ClO•, •Cl_2^-, and $O^{\bullet-}$ are relatively selective (Grebel et al., 2010). Since these radicals can induce synergistic micropollutant removal, the UV/chlorine reaction has

attracted significant interest, although disinfection products (DBPs) such as chloroform ($CHCl_3$) and chlorate (ClO_3) may form during the process (Fang et al., 2017; von Gunten, 2018).

Until now, the main UV sources for current UV-related AOP processes and disinfection are low- or medium-pressure mercury lamps (Chevremont et al., 2013a). Although these lamps are widely used in the water treatment system, there are still several issues with them. The major concern is that the UV lamps are fragile and contain toxic mercury, which is hazardous to the environment and requires proper disposal (Close et al., 2006; Chevremont et al., 2013b). Moreover, UV lamps require significant amounts of energy to operate due to a low wall-plug efficiency (WPE) (15-35%) and have a relatively short lifetime of about 10,000 h (Chatterley and Linden, 2010; Autin et al., 2013). In contrast, UV-LEDs which offer a variety of wavelengths are well aligned with the needs of efficient disinfection, making it a potential option (Song et al., 2016). UV-LED lamps have also several unique advantages such as environmental friendliness (no mercury), compactness and robustness (more durable), faster start-up time (no warm-up time), potentially less energy consumption, longer lifetime, and the ability to turn on and off with high frequency (Würtele et al., 2011). In addition, UV-LEDs can operate at 75% wall-plug efficiency with a lifetime longer than 100,000 h, comparable to the operating parameters of current visible LEDs (Autin et al., 2013; Ibrahim et al., 2014). If UV-LEDs/chlorine process combining UV-LED and chlorine is used to treat micropollutants, it can be energy-efficient and gives higher radical yields than the UV/H_2O_2 reaction at pH 6-7, due to the higher molar absorbance and quantum yields of hypochlorous acid (HOCl)

compared to hydrogen peroxide (Fang et al., 2014; Stefan, 2017; Yin et al., 2018; Zou et al., 2019).

1.2. Purpose of Research

In this study, we applied the UV-LED/chlorine process with various wavelengths (265 nm, 310 nm, and 365 nm) to investigate IPM degradation kinetics. The radical contribution depending on pH and wavelengths were examined. In addition, using the transformation products (TPs) using LC-Q-Tof/MS/Ms, the degradation pathway was proposed. Finally, the toxicity of IPM and its TPs were assessed along with EEO calculation.

Chapter 2. Materials and methods

2.1. Materials

Iopromide (IPM), sodium thiosulfate ($Na_2S_2O_3$), potassium phosphate monobasic (NaH_2PO_4), potassium phosphate dibasic (Na_2HPO_4), nitrobenzene (NB), benzoic acid (BA), 1,4-dimethoxybenzene (DMOB), and sodium hypochlorite solution (NaOCl) were purchased from Sigma-Aldrich (St. Louis, MO, USA). Free chlorine reagent (N, N-DPD (N, N-diethyl-p-phenylenediamine)) was obtained from Hach Co. (Loveland, CO, USA). All the chemicals used were of analytical grade.

2.2. UV-LED reactor

The schematic diagram of the UV-LED/chlorine system is shown in Fig. 1. We used a custom-made UV-LED apparatus (400W) emitting 265, 310, and 365 nm (CTLAB, Bundang, South Korea). The specification of the UV-LED lamp at each wavelength is shown in Table S1. The power of the UV-LED lamp was measured using UIT-250 photodetector(Ushio, Tokyo, Japan). The measured maximum power of the UV lamp was 16 mW cm^{-2} (265 nm), 41 mW cm^{-2} (310 nm), and 791 mW cm^{-2} (365 nm). To maintain the constant temperature from the heat emitted by high power UV-LED during the reaction, the reactor apparatus was cooled by a chiller (DSD-005N, Daeil, Pusan, Korea).

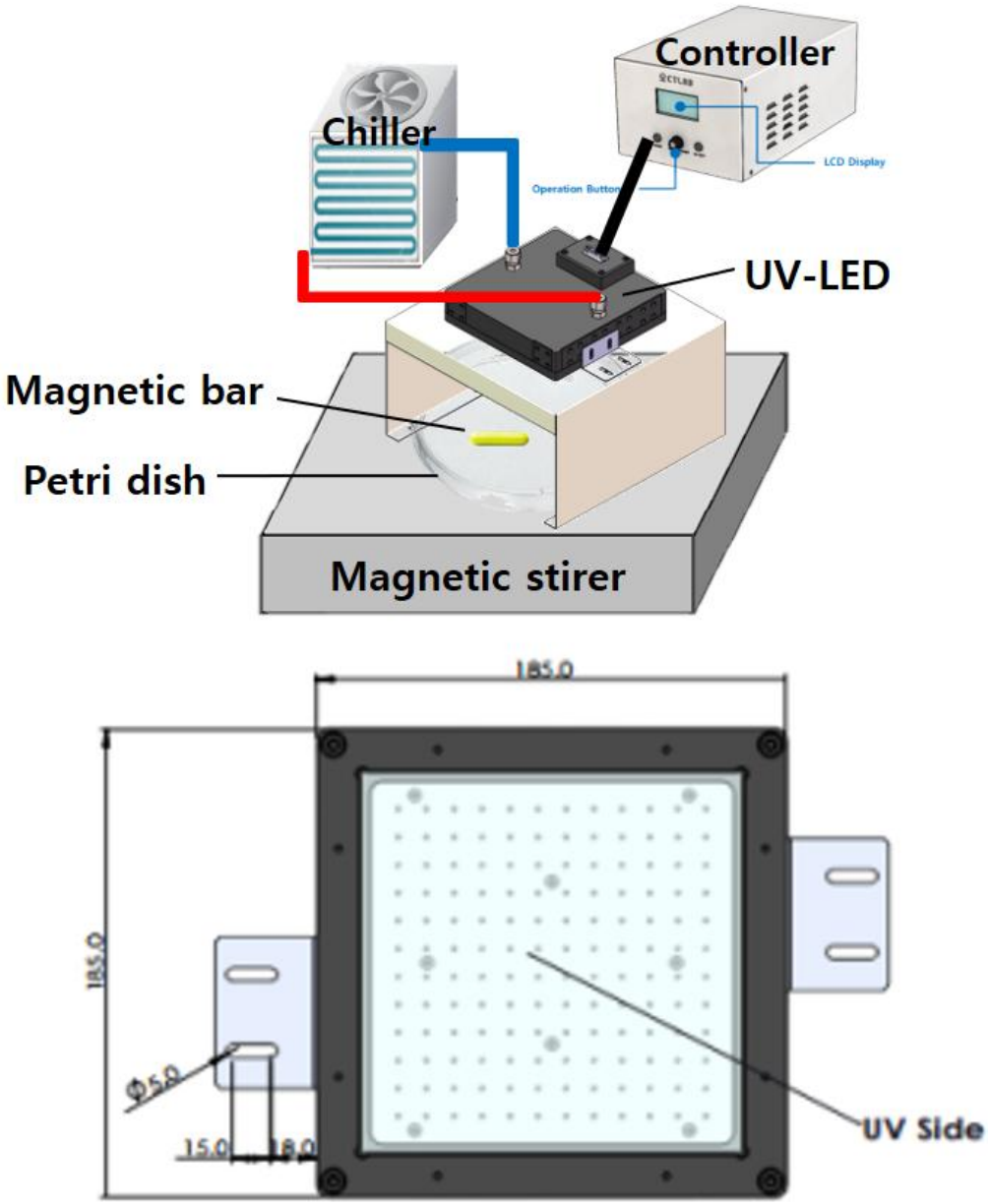

Fig. 1. The schematic diagram of the UV-LED reactor system

2.3. Experimental procedure

The fluence-dependent kinetic experiments of IPM degradation during dark chlorination, UV-LED photolysis, and UV-LED/chlorine reactions were conducted in a 100 mL glass petri dish. In the UV-LED (265 nm)/chlorine experiment, since the removal rate of IPM was very fast, the kinetic experiment was conducted by adjusting the power of UV-LEDs less than 10%. The effects of chlorine dosage (5-15 mg/L of chlorine) and pH (6 to 9) on IPM degradation were examined during the UV-LED/chlorine reaction. The pH of the reaction solution was maintained during the reactions with a 5 mM phosphate buffer solution. Since we used a high-output UV-LED lamp, we sampled every 5 - 30 seconds and all of the UV-LED/chlorine reactions were finished within 5 min. Residual chlorine was quickly quenched with 0.1 M $Na_2S_2O_3$ solution. All experiments were conducted twice and the R^2 of all data was higher than 0.995.

2.4. Analytical methods

We used ultra-high performance liquid chromatography quadrupole time-of-flight mass spectrometry (UPLC-QToF-MS) (ACQUITY UPLC System coupled with an SYNAPT G2-S mass spectrometer; Waters, Milford, MA, USA) with ACQUITY UPLC BEH C18 column (100 mm × 2.1 mm, 1.7 μM) to tentatively identify TPs during UV-LED/chlorine reactions. The detail of instrumental conditions of UPLC-QToF-MS is summarized in Table S2.

IPM, NB, BA, and DMOB were measured by using a Waters Xbridge column (PN:186003034, Waters, Milford, USA) with an HPLC-UV/VIS detector (UltiMate™

3000, Dionex, Sunnyvale, USA). The instrumental conditions in HPLC-UV/VIS for measurement of IPM, NB, BA, and DMOB are summarized in Table S3. The limit of quantitation (LOQ) of IPM, NB, BA, DMOB, and chlorine was 0.05, 0.01, 0.01, 0.01 and 0.01 mg/L respectively. The HPLC chromatograms of these compounds are shown in Fig. S1. Two peaks were found for IPM, and it was quantified using all of them because it was found to exist as two isomers (Putschew et al., 2007; Schulz et al., 2008).

Iodide was measured by ion chromatography (Dionex™ Aquion™ IC System., Thermo Scientific, Waltham, USA) coupled with the Ion Pac column (AS22, 4 × 250 mm). A guard column (AG22, 4 × 50 mm) was used to protect the main column. We prepared 4.8 mM Na_2CO_3/1.0 mM $NaHCO_3$ solution as eluent. The flow was 1.5 mL/min and set the current at 40mA. The detection limit of iodide in this method was 0.05 mg/L.

Total organic carbon (TOC) (TOC 5000; Shimadzu) was measured to evaluate the mineralization of IPM. The residual chlorine during the reaction was determined by Pocket Colorimeter (Hach Co.).

2.5. Toxicity assessment

The Microtox® (M500, Microbics Corp., Carlsbad, CA, USA) tests were employed to determine time-dependent acute toxicity trends during the UV-LED/chlorine reaction using the luminescent bacteria *V. fischeri* (NRRL number B-11177) based on the ISO 11348-3 standard protocol (Standardization, 2007). Packed in a 10-mL sealed vial, the test

organism was stored between -20°C and -25 °C, and the reconstitution solution, diluent (2% NaCl), and osmotic adjusting (OAS, 22% NaCl) solution were stored at room temperature. To prevent the osmotic effects of *V. fischeri*, all testing samples were adjusted to 2% NaCl using the OAS solution. *V. fischeri* was exposed to the treated solution for 15 min, and then we measured its luminescence intensity (L_t). The luminescence intensity of the control sample was also measured in a 3% NaCl solution (L_0). The toxicity removal rate was calculated based on the luminescence inhibition ($1 - L_t/L_0$).

To predict and calculate the toxicities of IPM and its TPs detected for fish, *daphnid*, and green algae, quantitative structure-activity relationship (QSAR) analysis was conducted using the Ecological Structure-Activity Relationship Model (ECOSAR, ver.2.0) (US EPA 2019) program.

Chapter 3. Results and discussion

3.1. IPM Degradation kinetics

We first examined the kinetics of IPM removal by UV-LED/chlorine at different pH and wavelengths (Fig. 2; Fig. 3; Table S4). IPM was removed more than 90% in 5 min at all wavelengths during UV-LED/chlorine reaction. For UV-LED/chlorine using 265 nm, the observed fluence-based rate constants for IPM (k'_{IPM}) increased in the order of pH 6, pH 7, and pH 8, but decreased sharply at pH 9. The reason for k'_{IPM} increases from pH 6 to pH 8 can be explained as follows; the rate constant ($k'_{chlorine}$) for chlorine decomposition by UV-LED photolysis increased as the pH increases so that it can produce more RCS, as

shown in Eqs. (1) – (7) (Fig. 4; Fig. 5). Changing pH can affect the abundance of HOCl and OCl^- (pK_a= 7.5), which are also radical scavengers for RCS in addition to being precursors of radical species (Fang et al., 2014) (Eq. (4)-(7)).

It is reported that micropollutants such as PPCPs can undergo proton transfer reactions to yield their protonated or deprotonated forms at varying pH, which may also affect their reactivity during the UV/chlorine reaction (Guo et al., 2017). Increasing pH from 6 to 9 can promote the transformation of IPM (pK_a = 9.9) from cationic to neutral forms which are richer in electrons so that the neutral form of IPM can be reactive with RCS. However, the k'_{IPM} decrease at pH 9 can be due to that the radical-scavenging effect of OCl^- ion is 2.7 - 4.4 times higher than that of HOCl (Eq. (4)-(7)) (Fang et al., 2017; Guo et al., 2017).

When using 310 nm and 365 nm LED, k'_{IPM} value decreased linearly as the pH increased in the order of pH 6, 7, 8, and 9 (Fig. 5(b) and 5(c)). This result is due to the radical-scavenging effect by OCl^- become greater than the generating effect of OH• and RCS as the pH increases (Fig. 5). Fig. 5 in section 3.3 showed the detailed k'_{IPM} data for each wavelength and pH.

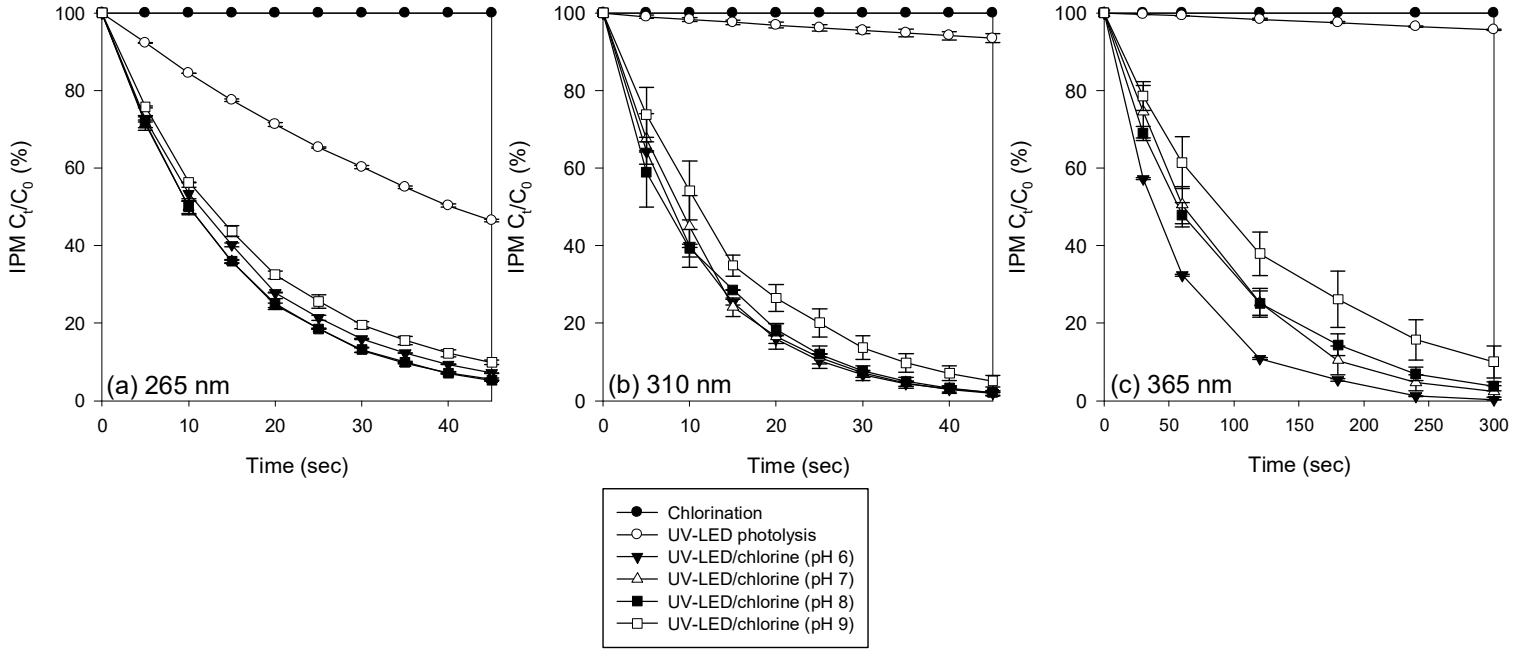

Fig. 2. Degradation of IPM by chlorination, UV-LED photolysis and UV-LED/chlorine process using 265 nm (1 $mWcm^{-2}$), 310 nm (41 $mWcm^{-2}$) and 365 nm (791 $mWcm^{-2}$) at different pH. $[IPM]_0$ = 10 μM, $[chlorine]_0$ = 10 mg/L, pH = 6, 7, 8, 9

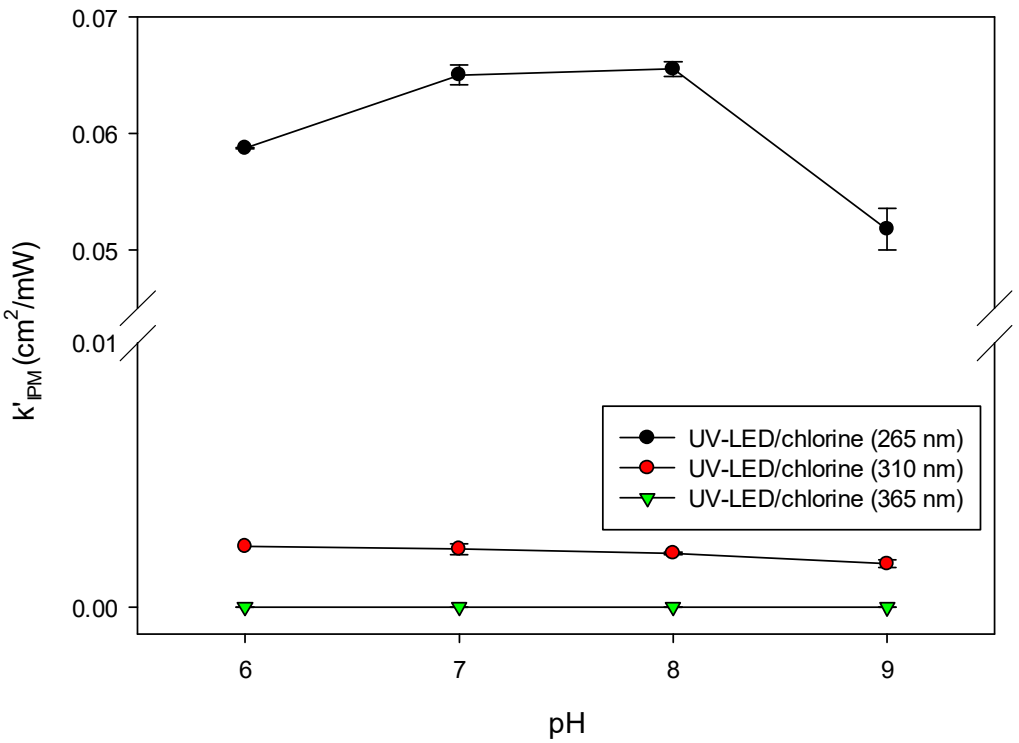

Fig. 3. Fluence-based rate constants of IPM degradation by UV-LED/chlorine process using 265 nm (1 $mWcm^{-2}$), 310 nm (41 $mWcm^{-2}$) and 365 nm (791 $mWcm^{-2}$) at different pH. $[IPM]_0$ = 10 μM, $[chlorine]_0$ = 10 mg/L, pH = 6, 7, 8, 9

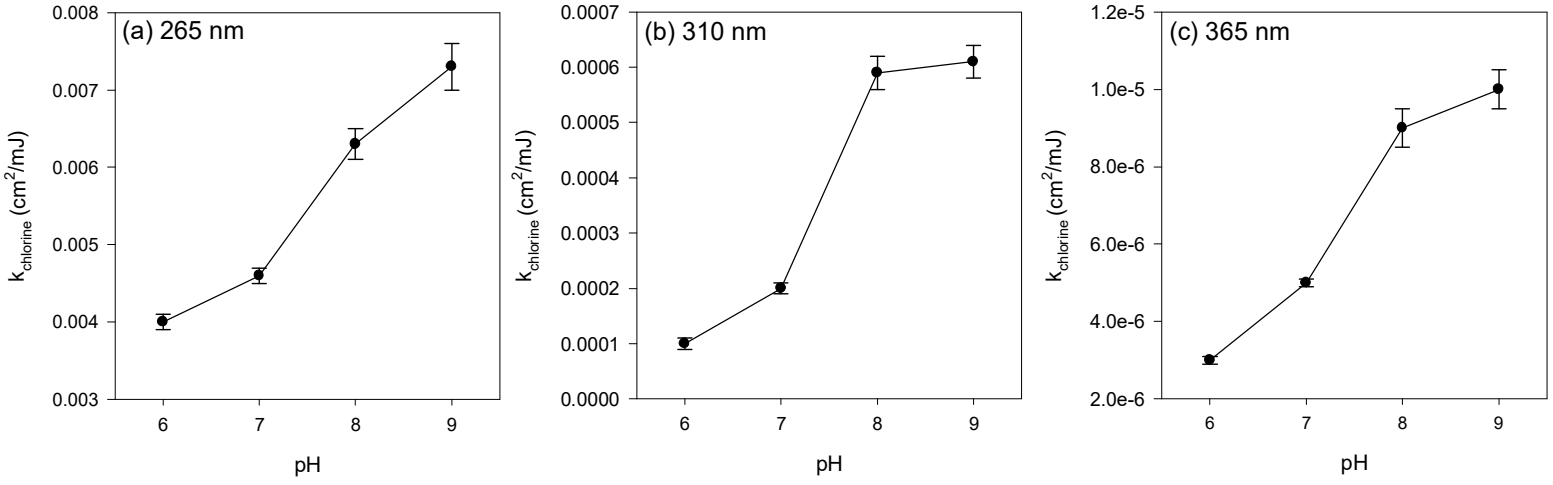

Fig. 4. Fluence-based rate constants of chlorine degradation by UV-LED/chlorine process using (a) 265 nm (1 $mWcm^{-2}$), (b) 310 nm (41 $mWcm^{-2}$) and (c) 365 nm (791 $mWcm^{-2}$) at different pH. $[chlorine]_0$ = 10 mg/L, pH = 6, 7, 8, 9.

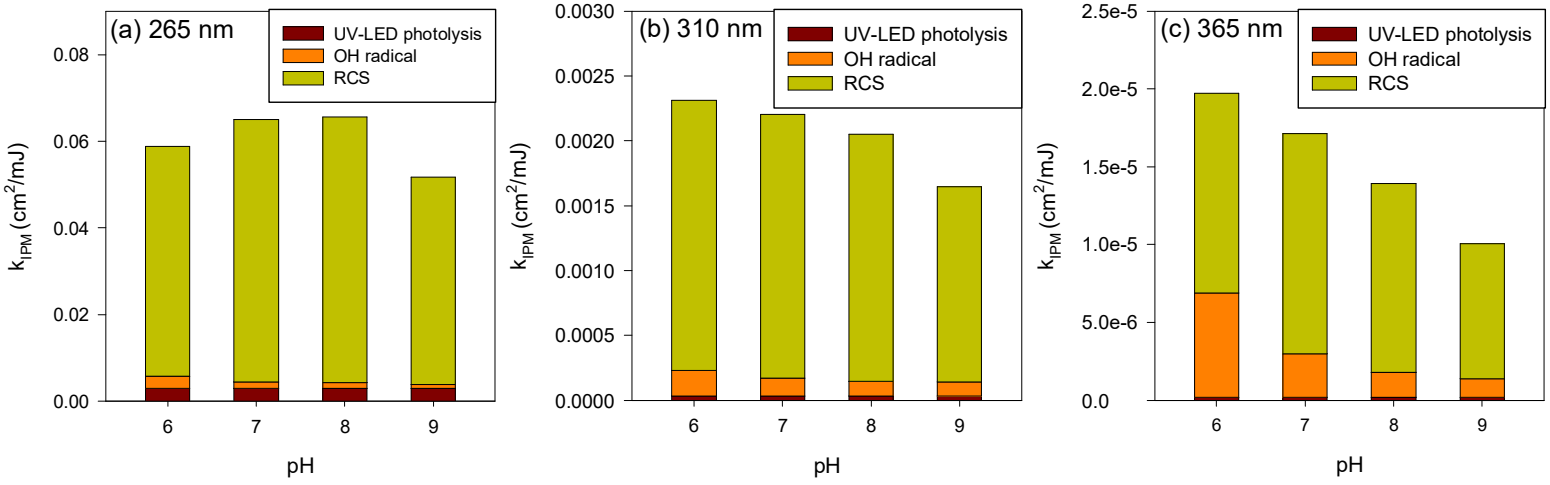

Fig. 5. Fluence-based rate constants of reactive species during IPM degradation by UV-LED/chlorine process using (a) 265 nm (1 $mWcm^{-2}$), (b) 310 nm (41 $mWcm^{-2}$) and (c) 365 nm (791 $mWcm^{-2}$) at different pH. $[IPM]_0$ = 10 μM, $[NB]_0$ = 10 μM, $[chlorine]_0$ = 10 mg/L, pH = 6, 7, 8, 9.

3.2. Effect of chlorine

The effect of chlorine dosage on the removal of IPM during the UV-LED/chlorine experiment was examined at 265 nm (Fig. 6). At a chlorine concentration of 3 mg/L or less, all chlorine was consumed before the IPM was completely removed. Therefore, only the date at the concentrations of 5, 10, 15 mg/L chlorine are shown in Fig. 3, and the detailed rate constants (k'_{IPM}) are shown in Table 1.

At pH 6, 7, and 8, the k'_{IPM} was saturated over 10 mg/L of chlorine, implying that excessive chlorine negatively affected IPM removal. However, the k'_{IPM} value increased linearly as the chlorine concentration increased from 5 to 15 mg/L at pH 9 ($R^2 = 0.997$) (Fig. 6). k'_{IPM} was the lowest at pH 9 at 5 and 10 mg/L of chlorine, but was greater than that of pH 6 at 15 mg/L of chlorine. This result is due to the radical-scavenging effect of OCl^- is higher than the effect of OH• and RCS generated at pH 9 under 10 mg/L of chlorine. In a previous study, the contribution of ClO• increased linearly with increasing chlorine dosage (Wu et al., 2017). This result implies that the k'_{IPM} value at pH 9 has the potential to increase drastically with additional chlorine addition. This is due that chlorine is dominant in the form of OCl^- under basic conditions, which is eventually reacts rapidly with OH• to form a ClO•, as shown in Eq. (5) (Sun et al., 2016). Also, this ClO radical was found to be the most influential species in IPM removal during UV-LED/chlorine process in this study (Fig. 7).

Table 1. Fluence-based rate constants during UV-LED/chlorine reaction at different chlorine dosage and pH. Wavelength= 265 nm (1 $mWcm^{-2}$), $[chlorine]_0$ = 0, 5, 10, 15 mg/L, pH = 6, 7, 8, 9

	Fluence-based rate constant (Unit: $cm^2\,mJ^{-1}$)			
	0 mg/L of Cl_2	5 mg/L of Cl_2	10 mg/L of Cl_2	15 mg/L of Cl_2
pH 6	2.85×10^{-3}	3.81×10^{-3}	5.88×10^{-3}	6.27×10^{-3}
pH 7		4.85×10^{-3}	6.51×10^{-3}	6.69×10^{-3}
pH 8		5.14×10^{-3}	6.56×10^{-3}	6.77×10^{-3}
pH 9		3.78×10^{-3}	5.18×10^{-3}	6.35×10^{-3}

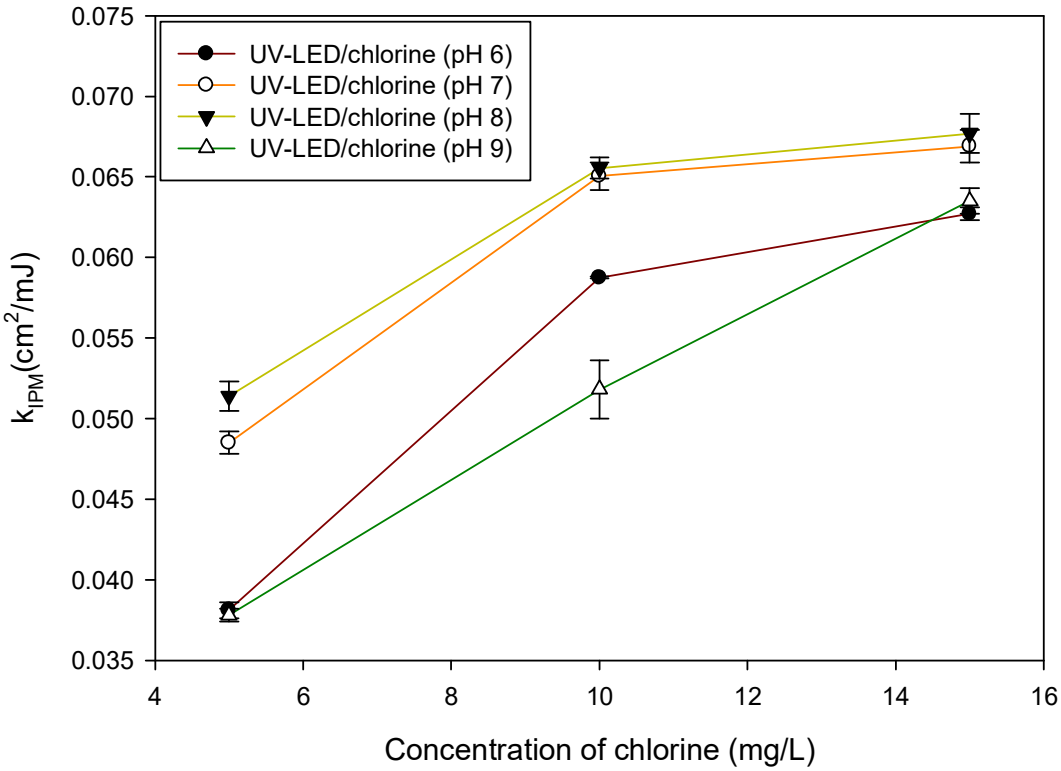

Fig. 6. Fluence-based rate constants of IPM degradation by UV-LED/chlorine process at different chlorine dosage and pH values. $[IPM]_0$ = 10 μM, $[chlorine]_0$ = 0 - 15 mg/L, pH = 6, 7, 8, 9, UV wavelength = 265 nm (1 mWcm^{-2})

3.3. Radical contribution

The radical contribution experiment was evaluated only for Cl•, and ClO• along with OH• because Cl•, and ClO• are expected to have relatively high removal contribution rates among various RCS (Hua et al., 2019; Kim et al., 2020). For calculating the contribution of these radical species during the UV-LED/chlorine reaction, we used NB, BA, and DMOB as radical scavengers. NB only reacts with OH• but not RCS, while BA is only reactive with OH• and Cl• (Fang et al., 2014), and DMOB reacts with OH•, Cl•, ClO• and ozone (Alfassi et al., 1988; Mvula et al., 2009; NIST, 2017). After removing the effect of ozone by nitrogen purging, $[OH•]_{SS}$, $[Cl•]_{SS}$, and $[ClO•]_{SS}$ can be calculated by Eqs. (8) to (10) using NB, BA, and DMOB.

$$k'_{NB} = k'_{d\text{-}NB} + k_{OH•,\,NB}[OH•]_{SS} \quad (8)$$

$$k'_{BA} = k_{OH,\,BA}[OH•]_{SS} + k_{Cl•,\,BA}[Cl•]_{SS} \quad (9)$$

$$k'_{DMOB} = k_{OH•,\,DMOB}[OH•]_{SS} + k_{Cl•,\,DMOB}[Cl•]_{ss} + k_{ClO•,\,DMOB}[ClO•]_{SS} \quad (10)$$

where k'_{NB}, k'_{BA}, and k'_{DMOB} represent the pseudo-first-order rate constant for the degradation of NB, BA, and DMOB by UV-LED/chlorine reaction, respectively. $[OH•]_{SS}$, $[Cl•]_{SS}$, and $[ClO•]_{SS}$ represent the steady-state concentrations of OH•, Cl•, and ClO•, respectively (Table S5). $k'_{d\text{-}NB}$ represents the pseudo-first-order rate constant of NB during direct photolysis. $k_{OH•,\,NB}$, $k_{OH•,\,BA}$ and $k_{Cl•,\,BA}$ represent the second-order rate constants for NB with OH•, BA with OH• and BA with Cl•, respectively, which were reported to be 3.9×10^9 $M^{-1}s^{-1}$, 5.9×10^9 $M^{-1}s^{-1}$ and 1.8×10^{10} $M^{-1}s^{-1}$ (Fang et al., 2014). $k_{OH•,\,DMOB}$, $k_{Cl•,}$

$_{DMOB}$ and $k_{ClO\bullet, DMOB}$ represent the second-order rate constant of DMOB reacting with OH•, Cl•, and ClO•, respectively, which were reported to be 7.0×10^9 $M^{-1}s^{-1}$, 1.8×10^{10} $M^{-1}s^{-1}$ and 2.1×10^9 $M^{-1}s^{-1}$ (Alfassi et al., 1988; NIST, 2017). After that, we can calculate the pseudo-first-order rate constant of radical species by Eqs. (11) to (13).

$$k'_{IPM - OH\bullet} = k_{IPM, OH\bullet}[OH\bullet]_{SS} \quad (11)$$

$$k'_{IPM - Cl\bullet} = k_{IPM, Cl\bullet}[Cl\bullet]_{SS} \quad (12)$$

$$k'_{IPM - ClO\bullet} = k_{IPM, ClO\bullet}[ClO\bullet]_{SS} \quad (13)$$

where $k'_{IPM - OH\bullet}$, $k'_{IPM - Cl\bullet}$ and $k'_{IPM - ClO\bullet}$ represent for the degradation of IPM by OH•, Cl•, and ClO•, respectively. $k_{IPM, OH\bullet}$, and $k_{IPM, Cl\bullet}$ represent the second-order rate constant for IPM with OH• and IPM with Cl•, respectively, which were reported to be 3.3×10^9 $M^{-1}s^{-1}$ and 2.75×10^{10} $M^{-1}s^{-1}$ (Jeong et al. 2010; Lei et al., 2019). $k_{IPM, ClO\bullet}$ represents the second-order rate constant for IPM with ClO• (1.25×10^9 $M^{-1}s^{-1}$; Fig. S2) which was determined by the Eqs. (14)

$$k'_{IPM} = k_{IPM, ClO\bullet} / k_{DMOB, ClO\bullet} \times k'_{DMOB} \quad (14)$$

Finally, the relative contribution of IPM degradation kinetics during the UV-LED/chlorine process can be expressed as Eqs. (15).

$$k'_{IPM} = k_{IPM,\,OH\bullet}[OH\bullet]_{SS} + k_{IPM,\,Cl\bullet}[Cl\bullet]_{SS} + k_{IPM,\,ClO\bullet}[ClO\bullet]_{SS} + k_{IPM,\,others}[others]_{SS} + k'_{UV\text{-}IPM} \quad (15)$$

Using these equations, we found k'_{IPM} by OH• during UV-LED/chlorine reaction in the presence of NB (Fig. 5; Table 2). As shown in Fig. 5, at 265 nm, k'_{IPM} value by RCS increased from pH 6 to 8, but decreased sharply at pH 9. On the other hand, k'_{IPM} by OH• was decreased linearly as pH increased. This trend is similar to the previous study which was conducted with diatrizoate and iopamidol (Kong et al., 2018; Hua et al., 2019). The reason for this is explained in section 3.1. When using 310 nm, k'_{IPM} by RCS and OH• was decreased linearly as pH increased. Also, in the case of using 365 nm, k'_{IPM} by OH• was decreased linearly as pH increased but k'_{IPM} by RCS was high in the order of pH 7 > pH 6 > pH 8 > pH 9. In all wavelengths, OH• was not dominant, and at lower pH and a longer wavelength, the higher contribution of OH• was observed in the UV-LED/chlorine reaction. In addition, it was found that the pH dependency of OH• increased as the wavelength increased.

Since the contribution rate of RCS is dominant as shown in Fig. 2, to identify RCS contribution in more detail, the contribution rates of Cl• and ClO• at pH 7 were additionally identified by a mixed system of NB, BA, and DMOB (Fig. 7). The k'_{IPM} by Cl• and ClO• at 265 nm were 3.94×10^{-3} $cm^2\,mJ^{-1}$ (6.1 %) and 5.38×10^{-2} cm^2mJ^{-1} (82.8 %) respectively, and at 310 nm, 9.19×10^{-5} $cm^2\,mJ^{-1}$ (4.2 %) and 1.75×10^{-3} $cm^2\,mJ^{-1}$ (79.5 %) respectively, and at 365 nm, 6.00×10^{-7} $cm^2\,mJ^{-1}$ (3.5 %), 1.17×10^{-5} $cm^2\,m\,J^{-1}$ (68.5 %) respectively. This result indicates that, as the wavelength increased, the contribution rates of Cl• and

ClO• gradually decreased, but the contribution rate of ClO• is still dominant at all wavelengths. This result is consistent with the results of previous studies in which they found that the contribution of OH• and Cl• for iopamidol removal in the UV-C/chlorine is negligible (Kong et al., 2018). Interestingly, we found that Cl• showed a higher contribution rate than OH• at 265 nm, but not 310 nm and 365 nm. The contribution from unknown radicals were found to be 4.3%, 8.4%, 10.5% for 265 nm, 310 nm, and 365 nm, respectively., indicating that the contribution of minor species such as ClOH•, Cl_2•$^-$, O^-• increase as the longer wavelength is used. Although $k_{IPM,\ ClO•}$ (1.25×10^9 $M^{-1}s^{-1}$) is lower than $k_{IPM,\ OH}$ (3.3×10^9 $M^{-1}s^{-1}$) and $k_{IPM,\ Cl•}$ (2.75×10^{10} $M^{-1}s^{-1}$), the reason for the high contribution rate of ClO• is due to that [ClO]ss is higher than [OH]ss and [Cl]ss (Table S5).

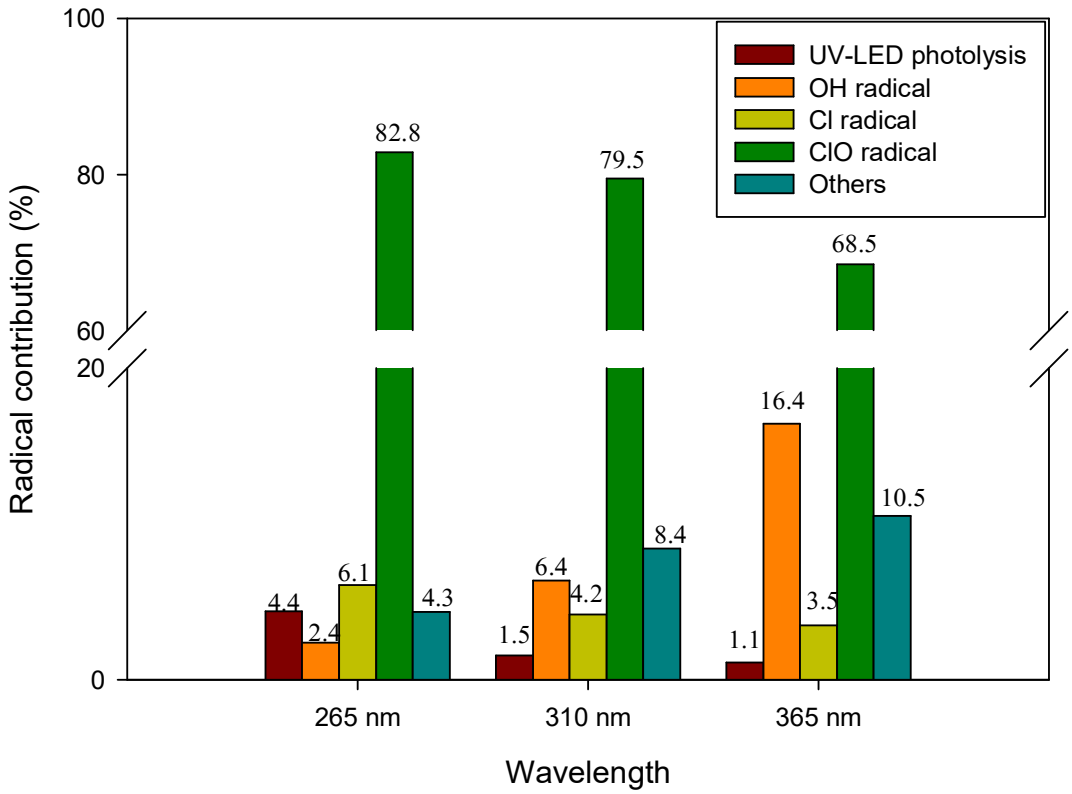

Fig. 7. Relative radical contribution (%) during UV-LED/chlorine process using 265 nm (1 $mWcm^{-2}$), 310 nm (41 $mWcm^{-2}$) and 365 nm (791 $mWcm^{-2}$). $[IPM]_0$ = 10 μM, $[NB]_0$ = 10 μM, $[BA]_0$ = 10 μM, $[DMOB]_0$ = 10 μM, $[chlorine]_0$ = 10 mg/L, pH = 7

Table 2. Fluence-based rate constants of radical species during UV-LED/chlorine reaction at different chlorine dosage and pH.

	265 nm	**310 nm**	**365 nm**
$k'_{IPM - OH\bullet}$ ($cm^2\ mJ^{-1}$)			
pH 6	2.82×10^{-3}	1.98×10^{-4}	6.71×10^{-6}
pH 7	1.54×10^{-3}	1.40×10^{-4}	2.81×10^{-6}
pH 8	1.37×10^{-3}	1.14×10^{-4}	1.62×10^{-6}
pH 9	9.42×10^{-4}	1.08×10^{-4}	1.19×10^{-6}
$k'_{IPM - RCS}$ ($cm^2\ mJ^{-1}$)			
pH 6	5.31×10^{-2}	2.07×10^{-3}	1.28×10^{-5}
pH 7	6.07×10^{-2}	2.02×10^{-3}	1.41×10^{-5}
pH 8	6.14×10^{-2}	1.90×10^{-3}	1.20×10^{-5}
pH 9	4.48×10^{-2}	$1.50 \times 10_{-3}$	8.67×10^{-6}
$k'_{IPM - UV}$ ($cm^2\ mJ^{-1}$)			
pH 6	2.85×10^{-3}	3.50×10^{-5}	2.00×10^{-7}
pH 7			
pH 8			
pH 9			

3.4. Energy efficiency evaluation dependent on irradiation wavelengths

To compare the energy efficiency among three wavelengths during the UV-LED/chlorine reaction, EEO (kwh m^{-3} $order^{-1}$) at different pH was calculated, and the wall plug efficiency (WPE) required for 310 nm, 3365 nm to achieve better energy efficiency than 265 nm was discussed. EEO is defined as the electric energy (kWh) required to decrease contaminant concentration per order of magnitude in a unit volume (1 m^3), which was calculated by Eq. (17) (derived from Eq. (15) and (16)) (Wang et al., 2017; Gao et al., 2019).

$$\mathrm{EEO} = \frac{1000Pt}{V \cdot \log(\frac{C_0}{C_t})} \tag{16}$$

$$P = \frac{IA}{10^6 \cdot \eta} \tag{17}$$

$$EEO = \frac{1000Pt}{V \cdot \log(\frac{C_0}{C_t})} \cdot \frac{IA}{10^6 \cdot \eta} = \frac{\ln(10) \cdot It}{\ln\left(\frac{C_0}{C_t}\right)} \cdot \frac{1000A}{10^6 \cdot \eta \cdot V} = \frac{0.64A}{10^6 \cdot \eta V k_{IPM}} \tag{18}$$

where P is the power on the water surface (kW), t is the irradiation time (h), V is the solution volume (0.1 L), C_0 and C_t are the concentration of IPM before and after UV irradiation (μM), I is the average UV irradiance on the water surface ($mWcm^{-2}$), A is the surface area of solution (122.72 cm^2), η is the WPE of the UV source (1.3% for 265 nm, 3.5% for 310 nm and 67.6% for 365 nm), and k'_{IPM} is the fluence-based rate constants of IPM degradation (cm^2mJ^{-1}).

As presented in Fig. 8, although the WPE of 310 nm and 365 nm was much higher than 265 nm, the EEO of 265 nm was much lower than others during UV-LED/chlorine reaction at all pH values. However, the synergistic effect of UV-LED and chlorine was greater at a higher wavelength (Table 3). In this experimental condition, even if WPE of 365 nm was increased to 100%, it was higher than EEO of 265 nm and 310 nm. However, in the case of UV-LED/chlorine using 310 nm, if WPE increase by about 30-40% or more, it can be lower than EEO of using 265 nm (Table 4). This experimental result has great implications for the possibility of using 310 nm UV-LED in the future.

Table 3. Comparison of EEO between UV-LED photolysis and UV-LED/chlorine reaction

	UV-LED photolysis	UV-LED/chlorine				EEO decrement
		pH 6	pH 7	pH 8	pH 9	
265 nm	21.20	1.03	0.93	0.92	1.17	18~23 times
310 nm	641.15	9.71	10.19	10.95	13.61	47~66 times
365 nm	5809.23	58.91	67.82	83.55	115.60	50~99 times

Unit: kWh/m^3/order

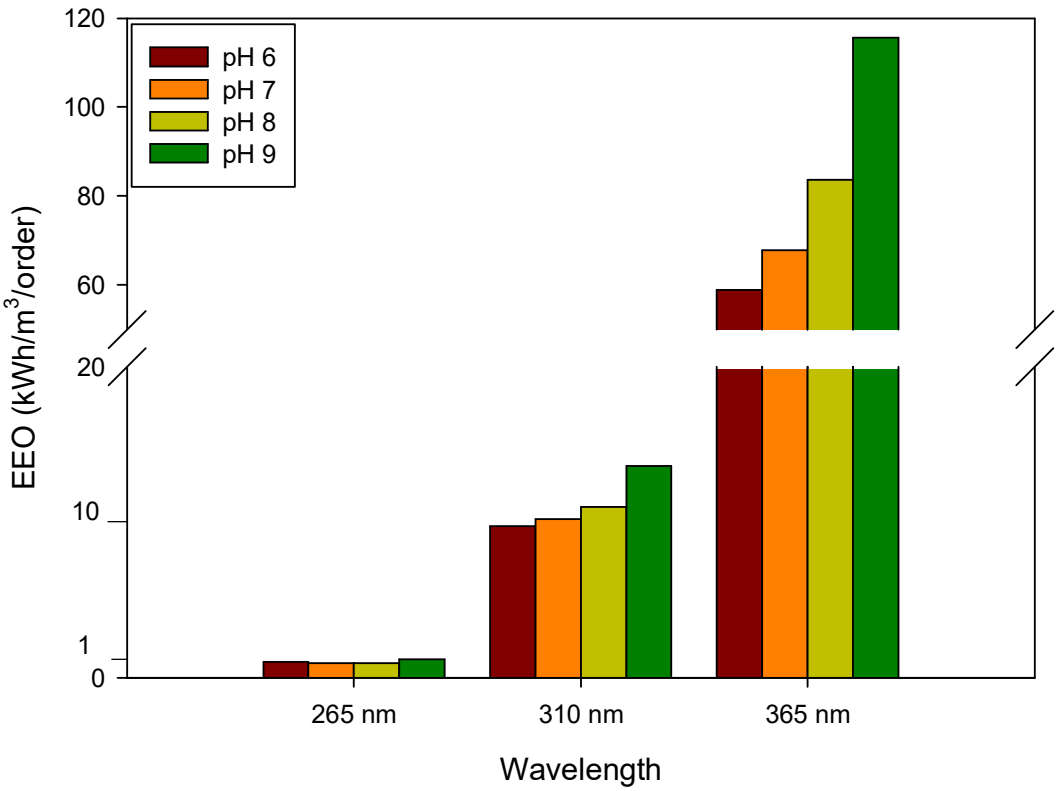

Fig. 8. EEO of IPM degradation by UV-LED/chlorine process using 265 nm (1 $mWcm^{-2}$), 310 nm (41 $mWcm^{-2}$) and 365 nm (791 $mWcm^{-2}$). $[IPM]_0$ = 10 μM, $[chlorine]_0$ = 10 mg/L, pH = 6, 7, 8, 9

Table 4. The ratios of EEO for UV-LED/chlorine using 310 nm to that for 265 nm and the target WPEs for 310 nm to achieve the same EEO as UV-LED/chlorine using 265 nm for IPM degradation by UV-LED/chlorine at different pH values.

	$EEO_{310\ nm}/EEO_{265\ nm}$ (kWh/m^3/order)	Target WPE (%)
pH 6	9.4	33.0
pH 7	11.0	38.4
pH 8	11.9	41.6
pH 9	11.7	40.8

3.5. Identified transformation products

We performed a UV-LED/chlorine experiment under the same conditions as the kinetic experiment. A total of nine tentative byproducts (mass error: ± 3 ppm) were identified (Fig. 9; Table 5). All the identified TPs were removed within 10 min, and among them, TP-699 was found in the UV-LED/chlorine process with all wavelengths (Fig. 10). TP-699 was produced by replacing I of the benzene ring with Cl, and it was confirmed that the response of the TP-699 increased as the lower wavelength is used. The maximum response of TP-699 at 265 nm, 310 nm, and 365 nm was 1926, 1229, and 992, respectively. TP-607 (Response: 200 – 300) is a form in which one more I is replaced with Cl in TP-699, and was only found in the UV-LED/chlorine reaction at using 265 nm. These results can prove that the contribution rate of RCS increases as the shorter wavelength.

The deiodination is known to occur easily through several advanced oxidation/reduction processes to other ICM (Jeong et al., 2010; Tian et al., 2014; Wendel et al., 2014; Gao et al., 2019). All other transformation byproducts (TP-789, TP-749, TP-747, TP-719, TP-717, TP-667, and TP-606) were induced by •OH because •OH can react easily with organics via one-electron oxidation, additions to unsaturated C-C bonds, and H abstraction (Buxton et al., 1988; Grebel et al., 2010). Subsequently, OH• and RCS played a key role in oxidizing amine to nitro groups by the cleavage of C-N bonds so that disinfection byproducts (DBPs) precursors can be produced (Shah and Mitch, 2012; Gao et al., 2019). The chromatograms of the detected TPs are shown in Table S6.

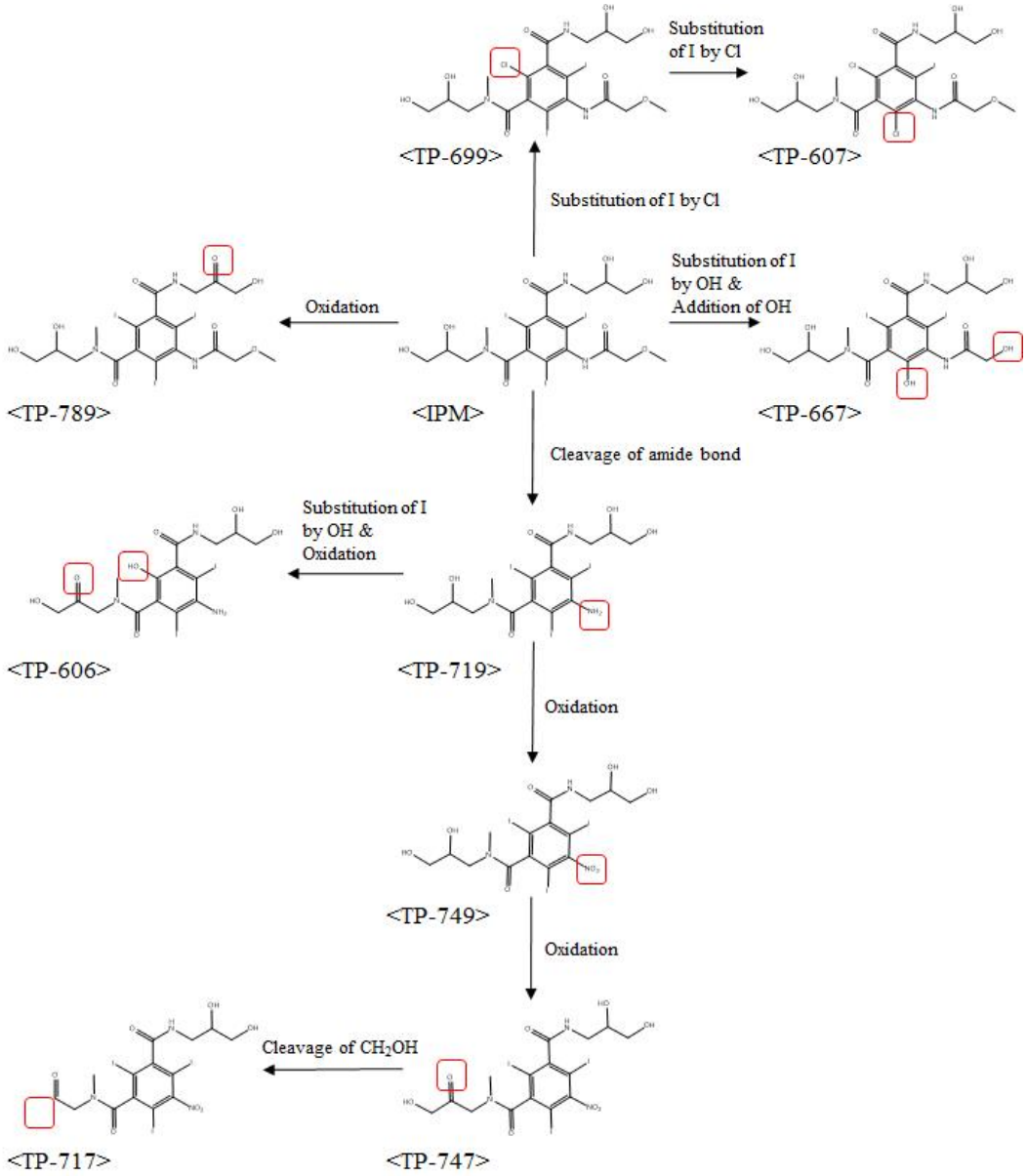

Fig. 9. Suggested degradation pathway of tentatively identified byproducts during UV-LED (265 nm)/chlorine. pH = 5.8 (distilled water), $[chlorine]_0$ = 1mg/L, $[IPM]_0$ = 1 μM

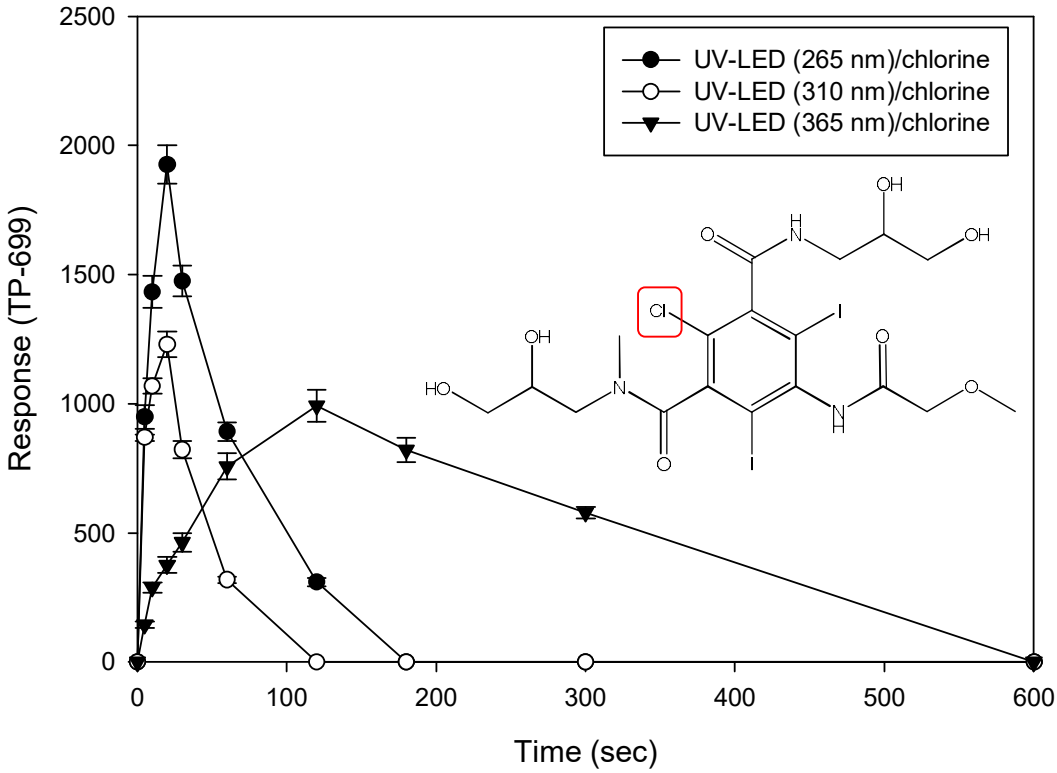

Fig. 10. Transformation byproducts (TP-699) during UV-LED/chlorine process using 265nm (1 $mWcm^{-2}$), 310 nm (41 $mWcm^{-2}$) and 365 nm (791 $mWcm^{-2}$). $[IPM]_0$ = 1 μM, $[chlorine]_0$ = 1 mg/L, pH = 5.8 (distilled water)

Table 5. Information of byproducts

Component	Formula	Expected mass (Da)	Observed m/z	Mass error (Da)	Mass error (ppm)	Observed RT (min)	Adducts	Reference
TP-789	$C_{18}H_{22}I_3N_3O_8$	788.8540	789.8625	-1.0	-1.3	2.6409	+ H	Singh et al., 2015
TP-749	$C_{15}H_{18}I_3N_3O_8$	748.8227	749.8314	-1.3	-1.8	3.0911	+ H	Wang et al., 2020
TP-747	$C_{15}H_{16}I_3N_3O_8$	746.8071	747.8173	-1.0	-1.3	3.0446	+ H	Wang et al., 2020
TP-719	$C_{15}H_{20}I_3N_3O_6$	718.8486	719.8575	-0.0	-0.0	2.7090	+ H	Wang et al., 2020
TP-717	$C_{14}H_{14}I_3N_3O_7$	716.8329	717.8377	-2.1	-2.9	2.7122	+ H	Wang et al., 2020
TP-699	$C_{18}H_{24}ClI_2N_3O_8$	698.9341	699.9436	0.1	0.1	2.6394	+ H	In this study
TP-667	$C_{17}H_{23}I_2N_3O_9$	666.9523	667.9600	0.4	0.6	5.9770	+ H	In this study
TP-607	$C_{18}H_{24}Cl_2IN_3O_8$	606.9985	608.0068	0.9	1.5	2.6377	+ H	In this study
TP-606	$C_{15}H_{19}I_2N_3O_7$	606.9312	606.9342	-0.7	-1.2	7.3063	- e	Singh et al., 2015

3.6. Acute toxicity evaluation

Although most of the parent compounds of ICM are known to have no toxicity, the transformation product of ICM can be risky to the ecosystem (Matsushita et al., 2015; Nowak et al., 2020). In particular, in the case of IPM, the luminescence inhibition rate of *V. fischeri* increased to 100% after the UV photolysis process (Fabbri et al., 2016). In this study, the ECOSAR (https://www.epa.gov/tsca-screening-tools/ecological-structure-activity-relationships-ecosar-predictive-model) was employed to evaluate the relative acute toxicities of IPM and TPs in various species. Software prediction is based on quantitative structure-activity relationships (Melnikov et al., 2016). LC_{50} doses (mg/L) were calculated for three different species (*Daphnia magna* (48 h), Green Algae (96 h), and fish (96 h)). Obtained data are summarized in Table 6. The result showed that the toxicity of TP-607, TP-667, and TP-699 was decreased compared to that of IPM at all species, while the toxicity of the other TPs was slightly increased. However, there were no TPs that showed significant toxicity.

V. fischeri luminescence inhibition test was performed to evaluate the mixture effect of treated water including unknown TPs during the UV-LED/chlorine process (Fig. 11). As a result of conducting the UV-LED/chlorine reaction with the maximum power, TOC result showed that the mineralization was achieved by more than 50% at all wavelengths. In addition, the initial luminescence inhibition of IPM was 20%, 19%, 22% at 265 nm, 310 nm, 365 nm, respectively, and the luminescence inhibition of the final treated water was found to to 27%, 23%, and 27%. Although there was a section where the inhibition was increased during the reaction at all wavelengths, it was found that the toxicity was not

significantly increased rather than the UV photolysis process that was previously studied (Fabbri et al., 2016).

Table 6. ECOSAR predicted acute toxicities (LC50, mg/L) for IPM and TPs using different models.

Compound	Fish (96 h)	Daphnid (48 h)	Green Algae (96 h)
IPM	7.05.E+05	1.35.E+06	1.66.E+04
TP-606	1.24.E+04	1.73.E+04	6.29.E+02
TP-607	3.55.E+06	7.97.E+06	5.72.E+04
TP-667	1.74.E+06	3.65.E+06	3.30.E+04
TP-699	1.59.E+06	3.31.E+06	3.11.E+04
TP-717	2.28.E+03	2.73.E+03	1.69.E+02
TP-719	5.38.E+04	8.38.E+04	2.10.E+03
TP-747	1.83.E+03	2.14.E+03	1.43.E+02
TP-749	1.50.E+04	2.09.E+04	7.64.E+02
TP-789	8.62.E+04	1.39.E+05	3.12.E+03

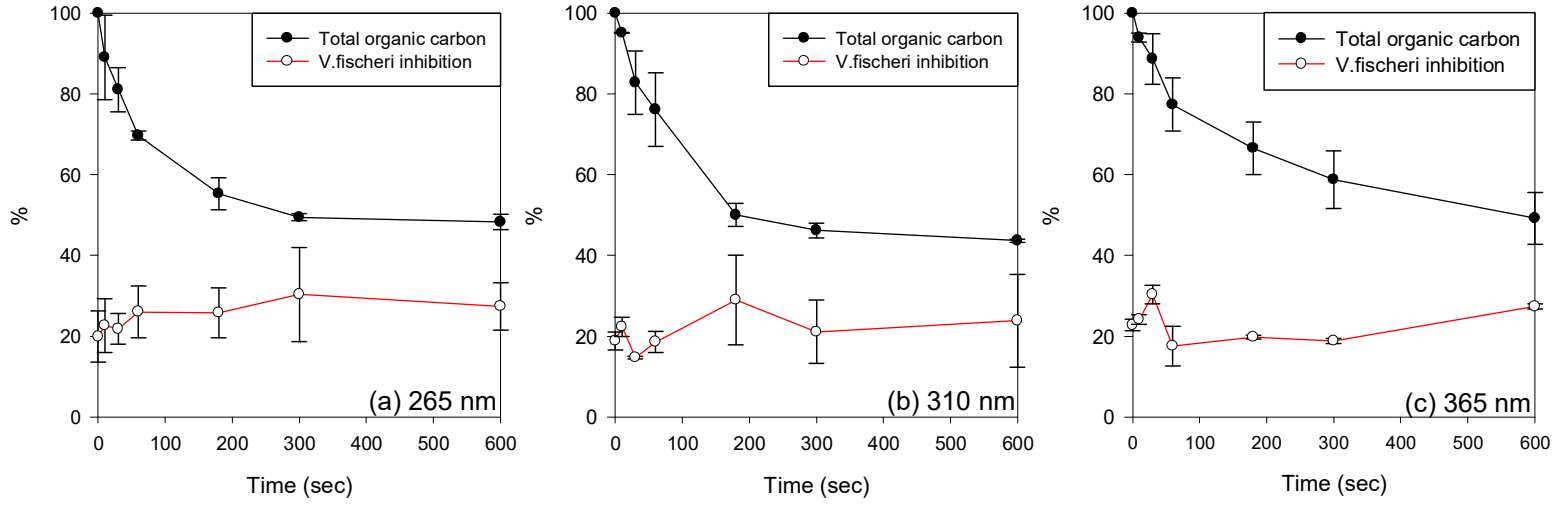

Fig. 11. *V.fischeri* luminescence inhibition and total organic carbon during UV-LED/chlorine process using (a) 265 nm (16 $mWcm^{-2}$), (b) 310 nm (41 $mWcm^{-2}$) and (c) 365 nm (791 $mWcm^{-2}$). $[IPM]_0$ = 10 μM, $[chlorine]_0$ = 10 mg/L, pH = 5.8 (distilled water)

3.6. Deiodination

In order to evaluate the deiodination efficiency, UV-LED/chlorine experiments were conducted for each wavelength (Fig 8). The theoretical iodide concentration of 10 μM IPM was 3.81 mg/L. When treated with the maximum power of each wavelength for 20 min, the final recoveries of 265 nm, 310 nm, and 365 nm were 43.2%, 30.6%, and 25.1%, respectively. Interestingly, when using 265 nm and 310 nm, there was a section where the concentration of iodide rapidly increased and then decreased at the beginning of the reaction, suggesting that the released iodide was regenerated into I-DBPs. Because residual iodide can participate in reactions involving heterogeneous chemical oxidation, reduction, which may eventually affect I-DBP levels (Dong et al., 2019). When using 310 nm, it is expected that more I-DBPs were generated than 265 nm and 365 nm because the concentration of iodide progressed more than 50% and then dropped to less than 20%. In particular, it is known that residual iodide is formed the most as iodate among I-DBPs (Li et al., 2017). Since I-DBPs such as iodoacetic acid and iodoacetamide are known to be almost always more cytotoxic and genotoxic than their chlorinated and brominated analogues (Li et al., 2017), it is necessary to study quantitative analysis and treatment methods for I-DBPs generated in the UV-LED/chlorine process.

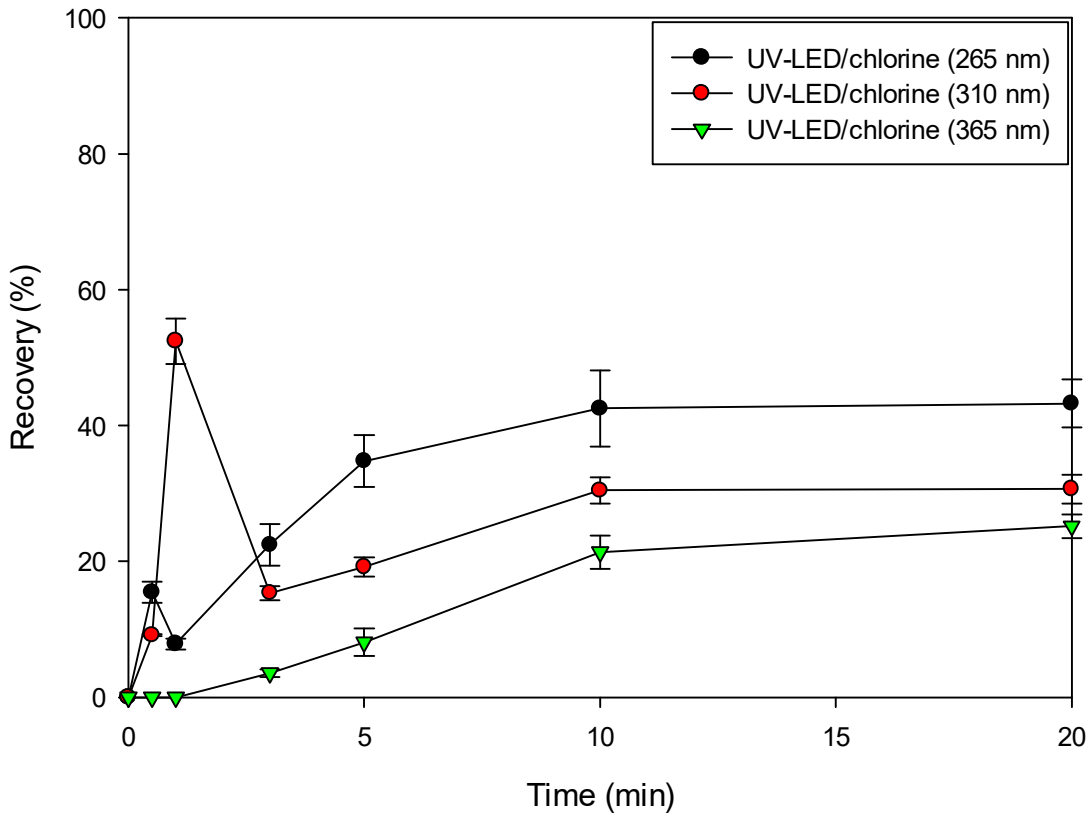

Fig. 12. Iodide release during UV-LED/chlorine process for IPM removal using 265 nm (16 $mWcm^{-2}$), 310 nm (41 $mWcm^{-2}$), and 365 nm (791 $mWcm^{-2}$) ($[IPM]_0$ = 10 μM, $[chlorine]_0$ = 10 mg/L, pH = 5.8 (distilled water))**.**

Chapter 4. Conclusions

The rate constant of IPM degradation (k'_{IPM}) in the UV-LED/chlorine reaction was in the order of 265 nm > 310 nm > 365 nm, and it was shown that over 90% was removed at all conditions. At 265 nm, k'_{IPM} value was in order of pH 8 > pH 7 > pH 6 > pH 9, however, k'_{IPM} decreased linearly as pH increased when using 310 nm and 365 nm. This is related to the change in the chemical properties of the IPM approaching the neutral form as the pH increases, and the change in the abundance of HOCl and OCl^-, which greatly affects the radical-scavenging effect. In the UV-LED/chlorine experiment by chlorine concentration using 265 nm, k'_{IPM} was saturated from 10 mg/L at pH 6, 7, 8. However, k'_{IPM} increased linearly as the chlorine concentration increased at pH 9. Further experiments are needed to determine the concentration of chlorine which makes saturates the k'_{IPM} at pH 9.

The contribution of OH• and RCS were examined using radical probe substances (NB, BA, DMOB) during UV-LED/chlorine reaction of IPM at various wavelengths and pH conditions. It was confirmed that RCS showed a larger contribution to IPM removal at short wavelengths than long wavelengths, and it was found that ClO• occupies the largest portion in RCS. The contribution of Cl• and OH• was relatively small at all wavelengths, however, the contribution of OH• increased as wavelength increased. It will be necessary to find out the contribution rates of the remaining unknown RCS such as ClOH•, $Cl_2^{\bullet-}$ for further study. From LC/Qtof/MS, nine TPs were identified, including three newly discovered TPs. Two of them are chlorinated TPs, and others are TPs generated by the attack of OH•. Through the response of TP-699, the radical contribution experiment for each wavelength was verified. Although the treated water including these TPs did not show

a toxicity increment in *V. fischeri* inhibition test, it is necessary to evaluate the eco-toxicity of the treated water through various indicators such as fish, *Daphnia magna*. Because it was confirmed that I-DBPs that can be cytotoxic and genotoxic can occur in the UV-LED/chlorine process through deiodination experiments.

In the case of UV-LED/chlorine using 310 nm, it can be more economical than using 265 nm when WPE is improved. Until now, it is difficult to apply UV-LED to the actual water treatment process right away because the WPE of LPUV (generally 20-30%) is better than that of UV-LED. However, the WPE and lifespan of UV-LEDs are predicted to increase to more than 75% and 100,000h, respectively, with a price drop of 40% so that eco-friendly UV-LED can be commercialized in the future.

Bibliography

Autin, O., Romelot, C., Rust, L., Hart, J., Jarvis, P., MacAdam, J., Parsons, S.A., Jefferson, B., 2013. Evaluation of a UV-light emitting diodes unit for the removal of micropollutants in water for low energy advanced oxidation processes. Chemosphere 92, 745-751.

Bettmann, M.A., 2004. Frequently asked questions: iodinated contrast agents. Radiographics 24, S3-S10.

Buxton, G.V., Greenstock, C.L., Helman, W.P., Ross, A.B., 1988. Critical review of rate constants for reactions of hydrated electrons, hydrogen atoms and hydroxyl radicals (· OH/· O− in aqueous solution. Journal of physical and chemical reference data 17, 513-886.

Chatterley, C., Linden, K., 2010. Demonstration and evaluation of germicidal UV-LEDs for point-of-use water disinfection. Journal of water and health 8, 479-486.

Chevremont, A.-C., Boudenne, J.-L., Coulomb, B., Farnet, A.-M., 2013a. Fate of carbamazepine and anthracene in soils watered with UV-LED treated wastewaters. water research 47, 6574-6584.

Chevremont, A.-C., Boudenne, J.-L., Coulomb, B., Farnet, A.-M., 2013b. Impact of watering with UV-LED-treated wastewater on microbial and physico-chemical parameters of soil. Water research 47, 1971-1982.

Close, J., Ip, J., Lam, K., 2006. Water recycling with PV-powered UV-LED disinfection. Renewable Energy 31, 1657-1664.
Dong, H., Qiang, Z., Richardson, S.D., 2019. Formation of iodinated disinfection byproducts (I-DBPs) in drinking water: emerging concerns and current issues. Accounts of chemical research 52, 896-905.
Fabbri, D., Calza, P., Dalmasso, D., Chiarelli, P., Santoro, V., Medana, C., 2016. Iodinated X-ray contrast agents: Photoinduced transformation and monitoring in surface water. Science of The Total Environment 572, 340-351.
Fang, J., Fu, Y., Shang, C., 2014. The roles of reactive species in micropollutant degradation in the UV/free chlorine system. Environmental science & technology 48, 1859-1868.
Fang, J., Zhao, Q., Fan, C., Shang, C., Fu, Y., Zhang, X., 2017. Bromate formation from the oxidation of bromide in the UV/chlorine process with low pressure and medium pressure UV lamps. Chemosphere 183, 582-588.
Gao, Z.-C., Lin, Y.-L., Xu, B., Xia, Y., Hu, C.-Y., Cao, T.-C., Zou, X.-Y., Gao, N.-Y., 2019. Evaluating iopamidol degradation performance and potential dual-wavelength synergy by UV-LED irradiation and UV-LED/chlorine treatment. Chemical Engineering Journal 360, 806-816.
Giri, P., Pal, C., 2014. Ecotoxicological aspects of pharmaceuticals on aquatic environment. American Journal of Drug Discovery 1, 10-24.
Grebel, J.E., Pignatello, J.J., Mitch, W.A., 2010. Effect of halide ions and carbonates on organic contaminant degradation by hydroxyl radical-based advanced oxidation processes in saline waters. Environmental science & technology 44, 6822-6828.
Guo, K., Wu, Z., Shang, C., Yao, B., Hou, S., Yang, X., Song, W., Fang, J., 2017. Radical chemistry and structural relationships of PPCP degradation by UV/chlorine treatment in simulated drinking water. Environmental science & technology 51, 10431-10439.
Hua, Z., Guo, K., Kong, X., Lin, S., Wu, Z., Wang, L., Huang, H., Fang, J., 2019. PPCP degradation and DBP formation in the solar/free chlorine system: Effects of pH and dissolved oxygen. Water research 150, 77-85.
Ibrahim, M.A., MacAdam, J., Autin, O., Jefferson, B., 2014. Evaluating the impact of LED bulb development on the economic viability of ultraviolet technology for disinfection. Environmental technology 35, 400-406.
Jennings, V.L., Rayner-Brandes, M.H., Bird, D.J., 2001. Assessing chemical toxicity with the bioluminescent photobacterium (Vibrio fischeri): a comparison of three commercial systems. Water research 35, 3448-3456.
Jeong, J., Jung, J., Cooper, W.J., Song, W., 2010. Degradation mechanisms and kinetic studies for the treatment of X-ray contrast media compounds by advanced oxidation/reduction processes. Water Research 44, 4391-4398.

Kläning, U.K., Wolff, T., 1985. Laser Flash Photolysis of HClO, ClO−, HBrO, and BrO− in Aqueous Solution. Reactions of Cl-and Br-Atoms. Berichte der Bunsengesellschaft für physikalische Chemie 89, 243-245.
Kong, X., Jiang, J., Ma, J., Yang, Y., Pang, S., 2018. Comparative investigation of X-ray contrast medium degradation by UV/chlorine and UV/H2O2. Chemosphere 193, 655-663.
Li, J., Jiang, J., Zhou, Y., Pang, S.-Y., Gao, Y., Jiang, C., Ma, J., Jin, Y., Yang, Y., Liu, G., 2017. Kinetics of oxidation of iodide (I−) and hypoiodous acid (HOI) by peroxymonosulfate (PMS) and formation of iodinated products in the PMS/I−/NOM system. Environmental Science & Technology Letters 4, 76-82.
Matsushita, T., Kobayashi, N., Hashizuka, M., Sakuma, H., Kondo, T., Matsui, Y., Shirasaki, N., 2015. Changes in mutagenicity and acute toxicity of solutions of iodinated X-ray contrast media during chlorination. Chemosphere 135, 101-107.
Matthew, B., Anastasio, C., 2006. A chemical probe technique for the determination of reactive halogen species in aqueous solution: Part 1–bromide solutions. Atmospheric Chemistry and Physics 6, 2423-2437.
Melnikov, F., Kostal, J., Voutchkova-Kostal, A., Zimmerman, J.B., Anastas, P.T., 2016. Assessment of predictive models for estimating the acute aquatic toxicity of organic chemicals. Green Chemistry 18, 4432-4445.
Nowak, A., Pacek, G., Mrozik, A., 2020. Transformation and ecotoxicological effects of iodinated X-ray contrast media. Reviews in Environmental Science and Bio/Technology 19, 337-354.
Pérez, S., Barceló, D., 2007. Fate and occurrence of X-ray contrast media in the environment. Analytical and bioanalytical chemistry 387, 1235-1246.
Putschew, A., Miehe, U., Tellez, A., Jekel, M., 2007. Ozonation and reductive deiodination of iopromide to reduce the environmental burden of iodinated X-ray contrast media. Water Science and Technology 56, 159-165.
Rastogi, T., Leder, C., Kümmerer, K., 2014. Qualitative environmental risk assessment of photolytic transformation products of iodinated X-ray contrast agent diatrizoic acid. Science of the Total Environment 482, 378-388.
Roberts, J., Kumar, A., Du, J., Hepplewhite, C., Ellis, D.J., Christy, A.G., Beavis, S.G., 2016. Pharmaceuticals and personal care products (PPCPs) in Australia's largest inland sewage treatment plant, and its contribution to a major Australian river during high and low flow. Science of the total environment 541, 1625-1637.
Schulz, M., Löffler, D., Wagner, M., Ternes, T.A., 2008. Transformation of the X-ray contrast medium iopromide in soil and biological wastewater treatment. Environmental science & technology 42, 7207-7217.
Sengar, A., Vijayanandan, A., 2021. Comprehensive review on iodinated X-ray contrast media: Complete fate, occurrence, and

formation of disinfection byproducts. Science of The Total Environment, 144846.
Seo, C.-D., Yoom, H.-S., Song, M.-J., Kim, K.-A., Kim, S.-Y., Son, H., 2020. Occurrence and Behavior of Residual Pharmaceuticals in the Nakdong River Basin. J. Korean Soc. Environ. Eng 42, 177-187.
Shah, A.D., Mitch, W.A., 2012. Halonitroalkanes, halonitriles, haloamides, and N-nitrosamines: a critical review of nitrogenous disinfection byproduct formation pathways. Environmental science & technology 46, 119-131.
Song, K., Mohseni, M., Taghipour, F., 2016. Application of ultraviolet light-emitting diodes (UV-LEDs) for water disinfection: A review. Water research 94, 341-349.
Standardization, I.O.f., 2007. Water Quality Determination of the Inhibitory Effect of Water Samples of the Light Emission of Vibrio Fischeri (luminiscent Bacteria Test). International Organization for Standardization-ISO.
Stefan, M.I., 2017. Advanced oxidation processes for water treatment: fundamentals and applications. IWA publishing.
Sun, P., Lee, W.-N., Zhang, R., Huang, C.-H., 2016. Degradation of DEET and caffeine under UV/chlorine and simulated sunlight/chlorine conditions. Environmental science & technology 50, 13265-13273.
Tian, F.-X., Xu, B., Lin, Y.-L., Hu, C.-Y., Zhang, T.-Y., Gao, N.-Y., 2014. Photodegradation kinetics of iopamidol by UV irradiation and enhanced formation of iodinated disinfection by-products in sequential oxidation processes. Water Research 58, 198-208.
von Gunten, U., 2018. Oxidation processes in water treatment: are we on track? Environmental science & technology 52, 5062-5075.
Wang, W.-L., Wu, Q.-Y., Li, Z.-M., Lu, Y., Du, Y., Wang, T., Huang, N., Hu, H.-Y., 2017. Light-emitting diodes as an emerging UV source for UV/chlorine oxidation: carbamazepine degradation and toxicity changes. Chemical Engineering Journal 310, 148-156.
Watts, M.J., Linden, K.G., 2007. Chlorine photolysis and subsequent OH radical production during UV treatment of chlorinated water. Water Research 41, 2871-2878.
Wendel, F.M., Lütke Eversloh, C., Machek, E.J., Duirk, S.E., Plewa, M.J., Richardson, S.D., Ternes, T.A., 2014. Transformation of iopamidol during chlorination. Environmental science & technology 48, 12689-12697.
Würtele, M., Kolbe, T., Lipsz, M., Külberg, A., Weyers, M., Kneissl, M., Jekel, M., 2011. Application of GaN-based ultraviolet-C light emitting diodes–UV LEDs–for water disinfection. Water research 45, 1481-1489.
Wu, M., Xiang, J., Que, C., Chen, F., Xu, G., 2015. Occurrence and fate of psychiatric pharmaceuticals in the urban water system of Shanghai, China. Chemosphere 138, 486-493.
Wu, Z., Guo, K., Fang, J., Yang, X., Xiao, H., Hou, S., Kong, X., Shang, C., Yang, X., Meng, F., 2017. Factors affecting the roles of reactive species in the degradation of micropollutants by the UV/chlorine process. Water research 126, 351-360.

Yin, R., Ling, L., Shang, C., 2018. Wavelength-dependent chlorine photolysis and subsequent radical production using UV-LEDs as light sources. Water research 142, 452-458.
Zehavi, D., Rabani, J., 1972. Oxidation of aqueous bromide ions by hydroxyl radicals. Pulse radiolytic investigation. The Journal of Physical Chemistry 76, 312-319.
Zhang, S., Gitungo, S., Dyksen, J.E., Raczko, R.F., Axe, L., 2021. Indicator Compounds Representative of Contaminants of Emerging Concern (CECs) Found in the Water Cycle in the United States. International journal of environmental research and public health 18, 1288.
Zou, X.-Y., Lin, Y.-L., Xu, B., Zhang, T.-Y., Hu, C.-Y., Cao, T.-C., Chu, W.-H., Pan, Y., Gao, N.-Y., 2019. Enhanced ronidazole degradation by UV-LED/chlorine compared with conventional low-pressure UV/chlorine at neutral and alkaline pH values. Water research 160, 296-303.

국문초록

요오드계 조영제의 일종인 iopromide(IPM)는 환경부 지정 1 순위 난분해성 물질로 폐수처리장에서 높은 농도로 검출되는 실정이다. IPM 은 염소에 전혀 반응하지 않고 OH 래디컬과도 상대적으로 반응성이 적기 때문에 다량의 활성염소종을 발생시키는 UV-LED/chlorine 공정을 적용하는 것이 효율적일 수 있다. 본 연구에서는 세 파장(265 nm, 310 nm, 365 nm)을 사용하여 UV-LED/chlorine 실험을 진행하여 효율성 및 제거 메커니즘을 정량적으로 비교, 평가하였다. Fluence-based rate constant (k_{IPM}')는 조사 파장이 증가함에 따라 감소하였지만, UV-LED 와 염소의 시너지 효과는 365 nm 에서 가장 컸다. 265 nm 을 사용한 경우는 pH 8 > pH 7> pH 6 > pH 9 순으로 k_{IPM}'가 컸고 310 nm 과 365 nm 는 모두 pH 가 증가할수록 k_{IPM}'가 일정하게 감소하였다. 활성염소종과 OH 래디컬의 기여도를 확인하기 위해 nitrobenzene, benzoic acid, 1,4-dimethoxybenzene 을 프로브 물질로 사용하였다. 활성염소종은 파장이 증가함에 따라 기여도가 감소하였고 OH 래디컬은 증가하였다. 또한 이번 실험 결과로 활성염소종 중 가장 많은 기여율을 차지하는 종은 ClO 래디컬인 것으로 밝혀졌다. LC-qToF/MS 를 이용하여 UV-LED/chlorine 공정 중 발생하는 소독부산물 9 개를 특정하였고, 이 중 염소화 부산물인 TP-699 가 짧은 파장에서 더 많이 생성되는 것 확인하였다. 이들 소독부산물의 mixture effect 를 확인하기 위해 *Vibrio fischeri* 발광 저해도 실험을 진행하였고 초기 독성 대비 최종 처리수의 독성 증가율은 모두 10%이내였다.

Supplementary Information

Degradation mechanisms of iopromide during the UV-LEDs/chlorine reaction

Table of contents

Table S1. Specification of UV-LED (400W) system.

	LAMP (mW/cm^2)		
Power (%)	365 nm	310 nm	265 nm
100	791	41	16
90	717	36	14
80	642	31	12
70	568	25	10
60	493	19	9
50	419	-	7
40	333	-	6
30	246	-	4
20	160	-	3
10	73	-	1

Table S2. Analysis conditions of UPCL-qTOF/MS for organic byproducts of IPM.

Instrument		Parameter	Condition
UPLC-qTOF/MS*	UPLC	Column	Waters, ACQUITY UPLC BEH C18 (100mm × 2.1 mm, 1.7 μm) (A) 0.1% formic acid in deionized water (B) Acetonitrile
		Mobile phase	Gradient mode, (A): (B) (v/v) = 98: 2(0min)->98:2(1min)->2:98(4.5min)- >2:98(7.60min)->98:2(10min)
		Flow rate	0.3 mL/min
		Injection volume	10 μL
		Column temperature	40℃
	qTOF/MS	Ionization mode	ESI positive
		Mass range	50-1200 Da
		Scan time	0.5 sec
		Collision energy	(Trap) 6 eV, (Ramp trap) 20-45 eV
		Capillary voltage	3.0 kV
		Source temperature	100 °C
		Sampling cone voltage	30 V
		Source offset	80 V
		Desolvation temperature	250 °C
		Cone gas flow	0 L/h
		Desolvation gas flow rate	800 L/h
		Nebulizer gas flow	6.5 bar

*

Table S3. Instrumental conditions of HPLC-UV/VIS

	Iopromide	Nitrobenzene	Benzoic acid	1,4-dimethoxybenzene
Flow rate (mL/min)	1.0	1.0	1.0	0.5
Eluent A (0.1% formic acid in distilled water)	94 %	40 %	40 %	-
Eluent B (Distilled water)	-	-	-	40 %
Eluent C (Aceotnitirle)	6 %	-	-	-
Eluent D (Methanol)		60 %	60%	60 %
Wavelength	238 nm	262 nm	230 nm	278 nm
Column	Waters Xbridge column (PN:186003034, Waters, Milford, USA)			
Column temperature	30 ℃			

Table S4. Fluence-based rate constants of IPM degradation by UV-LED/chlorine process. $[IPM]_0$ = 10 μM, $[chlorine]_0$ = 10 mg/L

	Fluence-based rate constant (Unit: cm^2 mJ^{-1})		
	265 nm	**310 nm**	**365 nm**
pH 6	5.87×10^{-2}	2.31×10^{-3}	1.97×10^{-5}
pH 7	6.50×10^{-2}	2.20×10^{-3}	1.71×10^{-5}
pH 8	6.55×10^{-2}	2.05×10^{-3}	1.39×10^{-5}
pH 9	5.18×10^{-2}	1.65×10^{-3}	1.00×10^{-5}

Table S5. Observed steady-state radical species (OH•, Cl• and ClO•) concentration (M) during the UV-LED/chlorine.

	265 nm	**310 nm**	**365 nm**
$[OH•]_{ss}$			
pH 6	8.5E-13	2.4E-12	1.9E-12
pH 7	4.6E-13	1.7E-12	6.7E-13
pH 8	4.1E-13	1.4E-12	3.8E-13
pH 9	2.8E-13	1.3E-12	2.8E-13
$[Cl•]_{ss}$			
pH 7	1.4E-13	1.4E-13	1.7E-14
$[ClO•]_{ss}$			
pH 7	4.3E-11	1.0E-12	7.43E-12

Table S6. Identified transformation byproducts of IPM during UV-LED/chlorine reaction.

Byproduct
TP-789
Structure 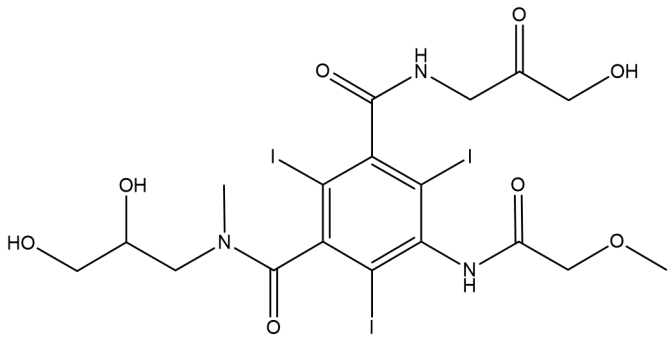   Chromatogram 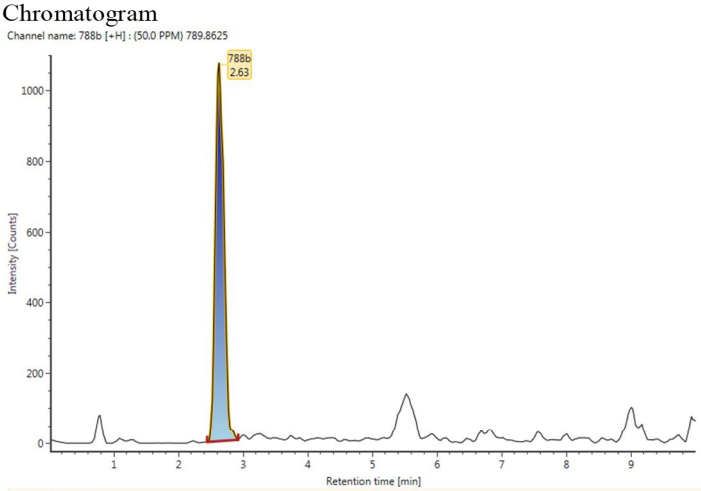   Item description: 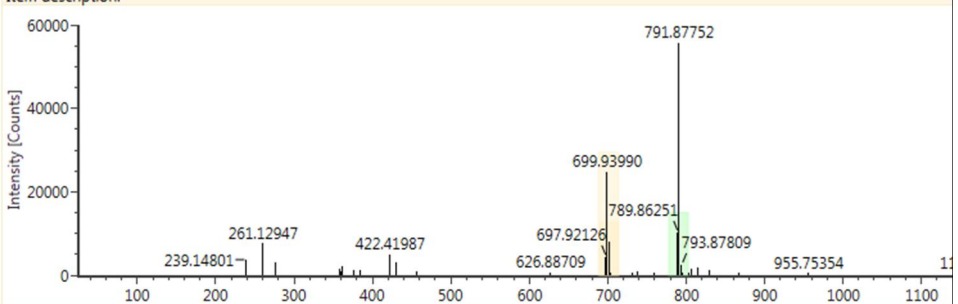

Byproduct
TP-749

Structure

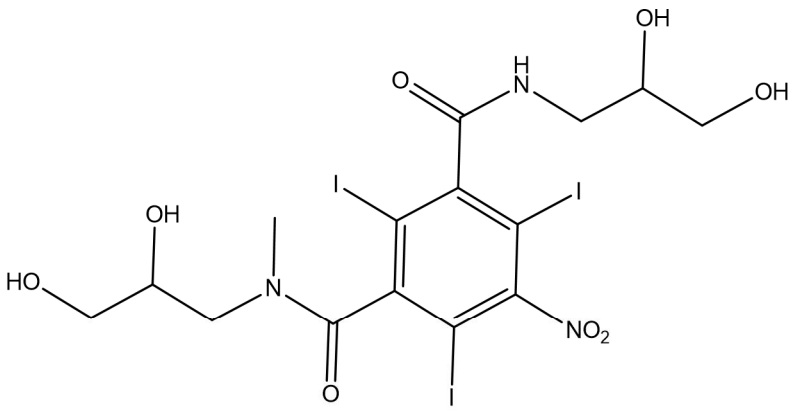

Chromatogram

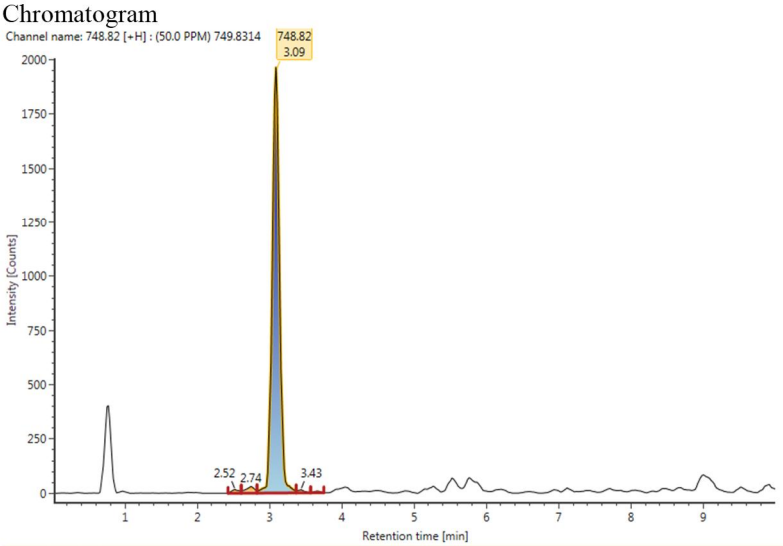

Item description:

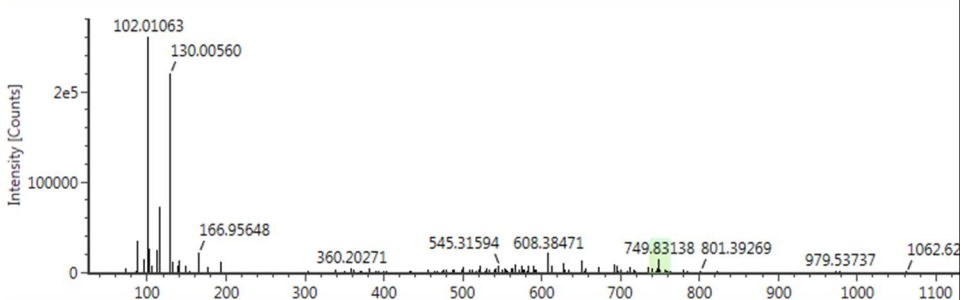

Byproduct
TP-747

Structure

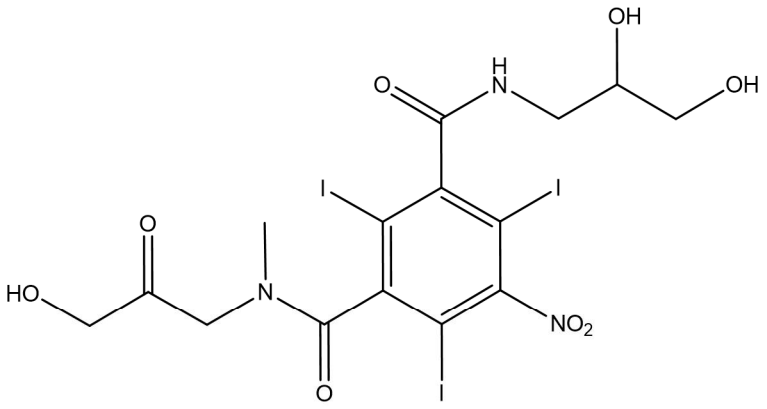

Chromatogram

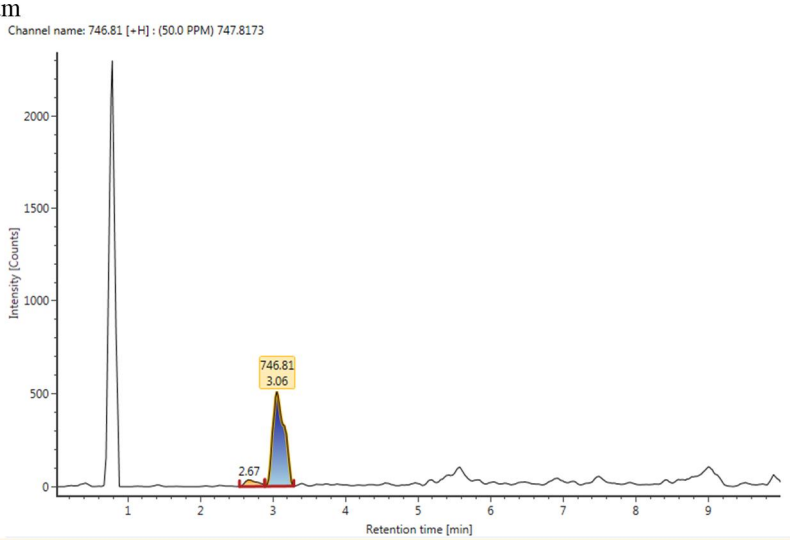

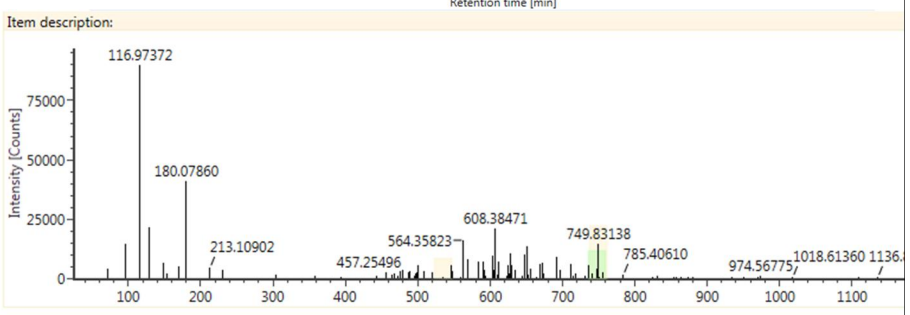

Byproduct
TP-719

Structure

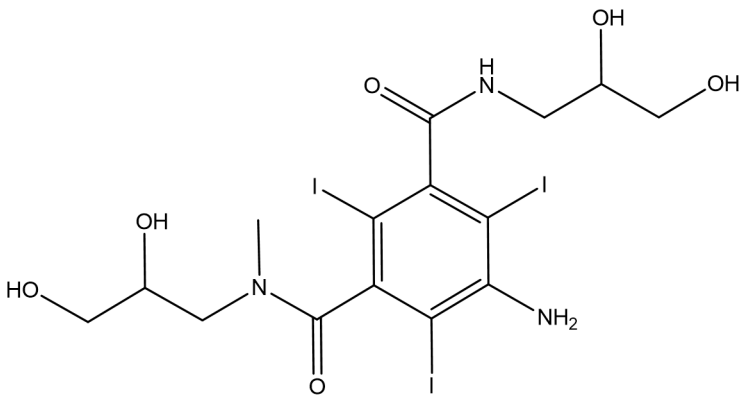

Chromatogram

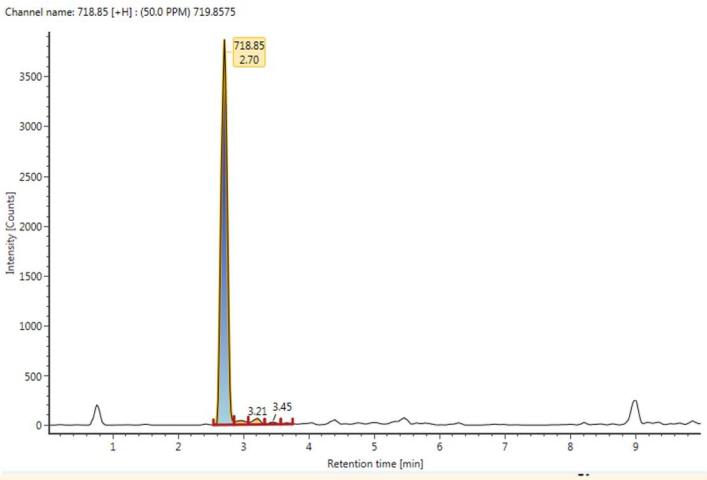

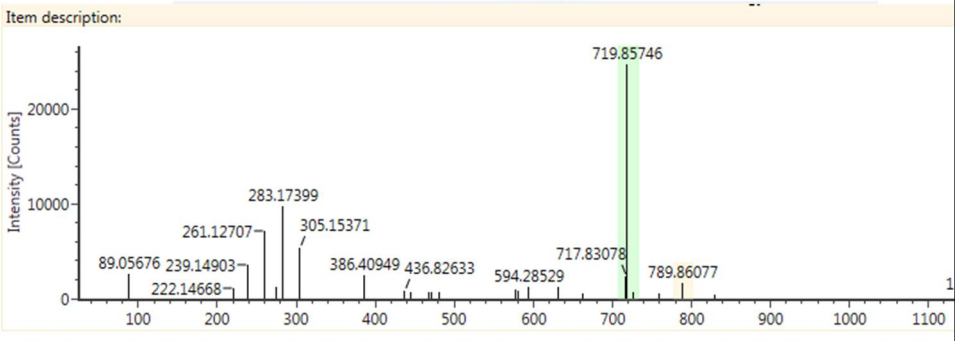

Byproduct
TP-717

Structure

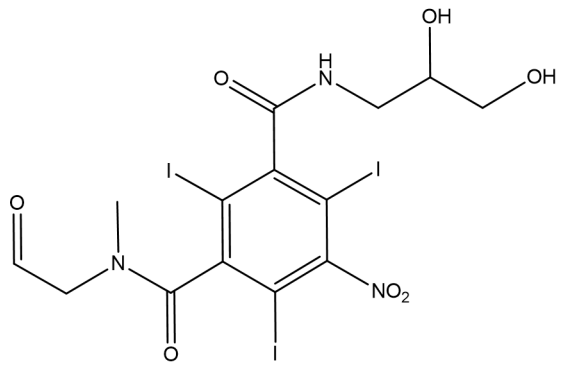

Chromatogram

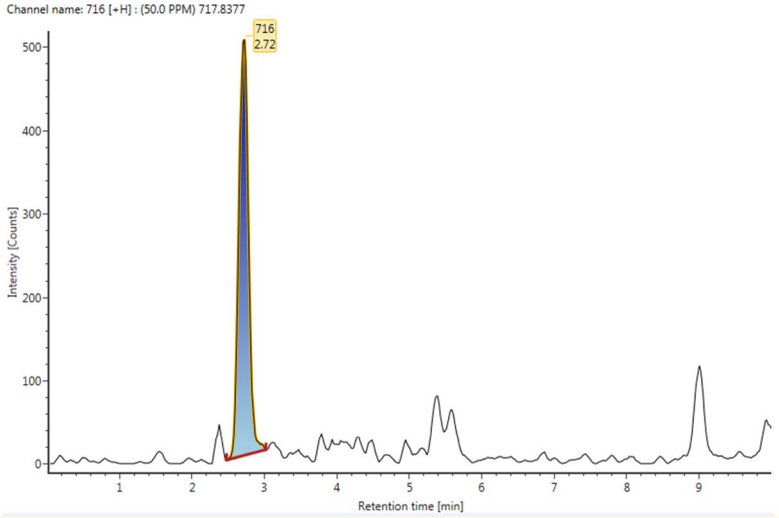

Item description:

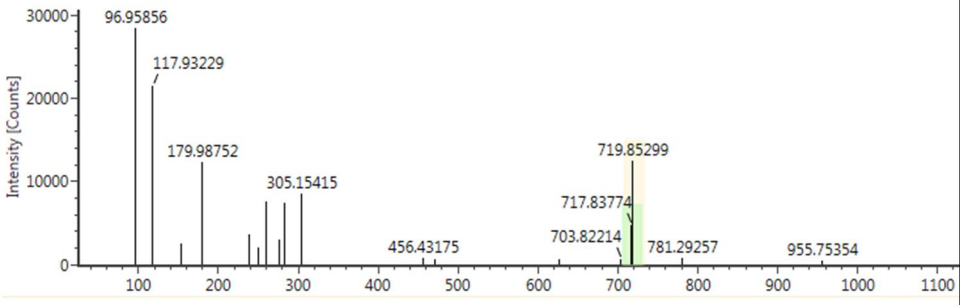

Byproduct
TP-699

Structure

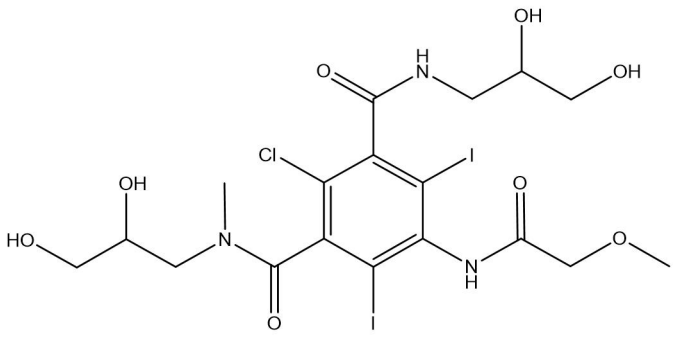

Chromatogram

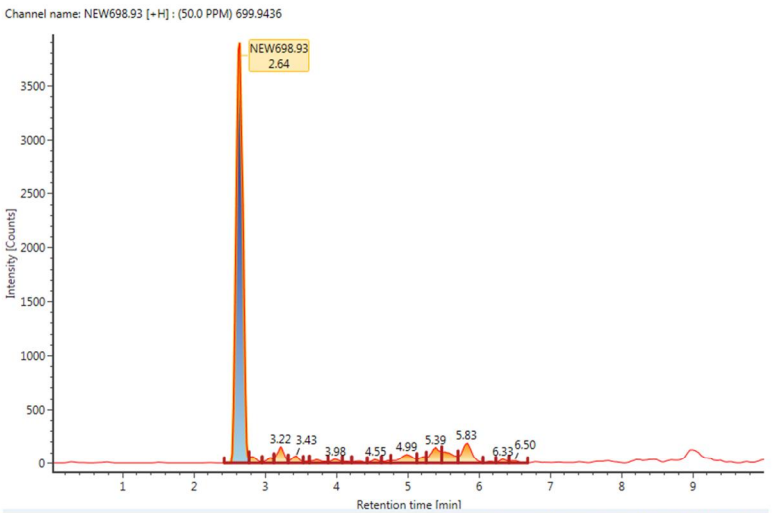

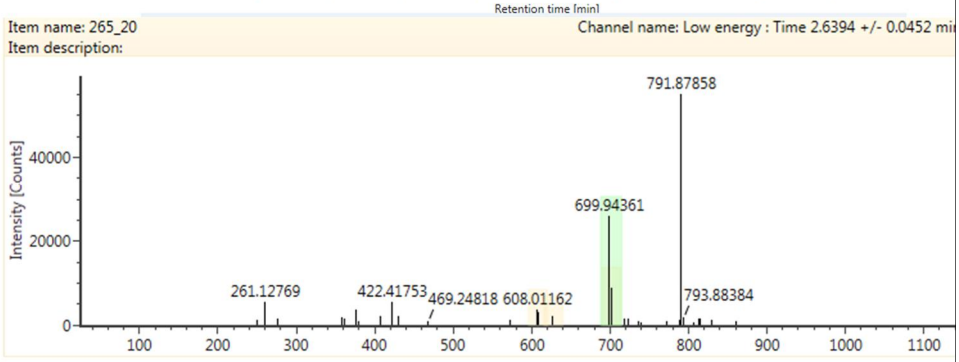

Byproduct
TP-667

Structure

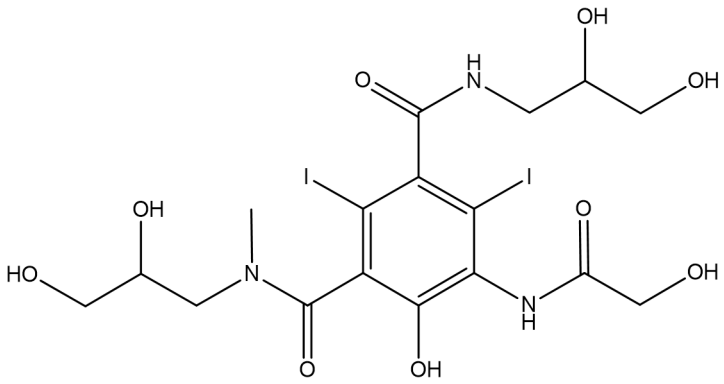

Chromatogram

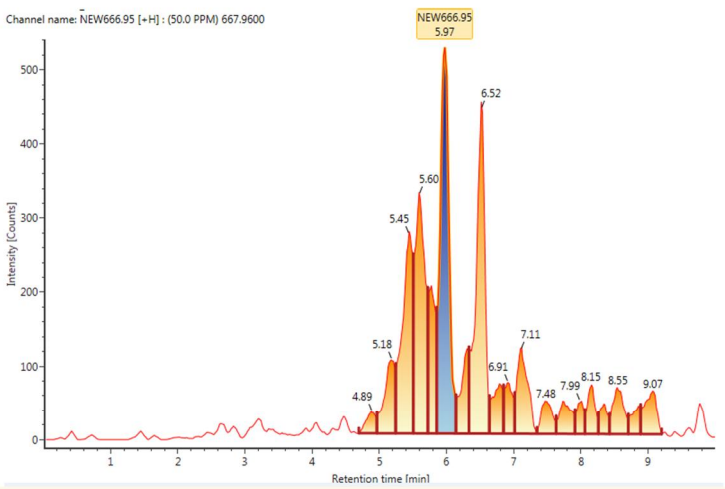

Item description:

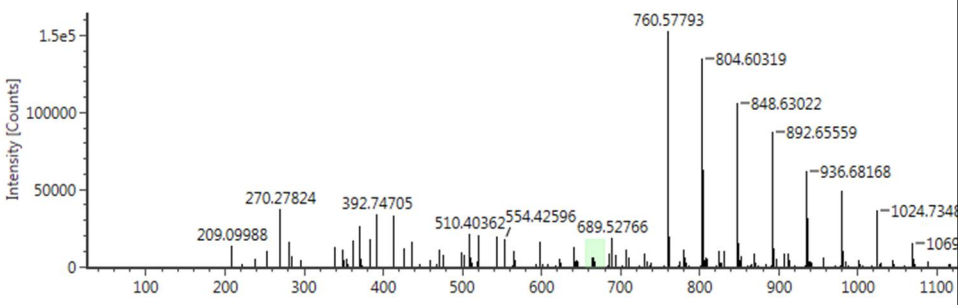

Byproduct
TP-607

Structure

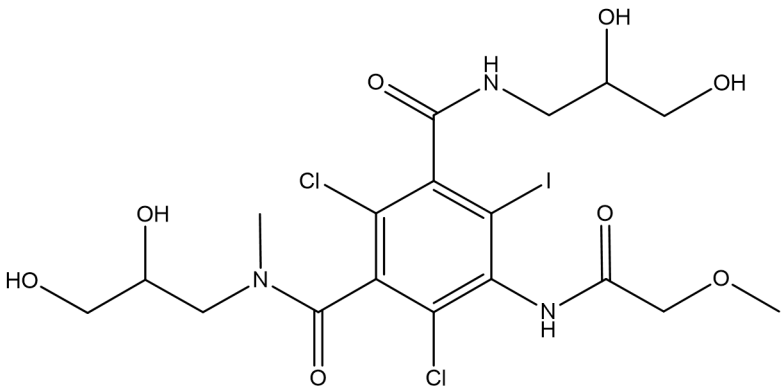

Chromatogram

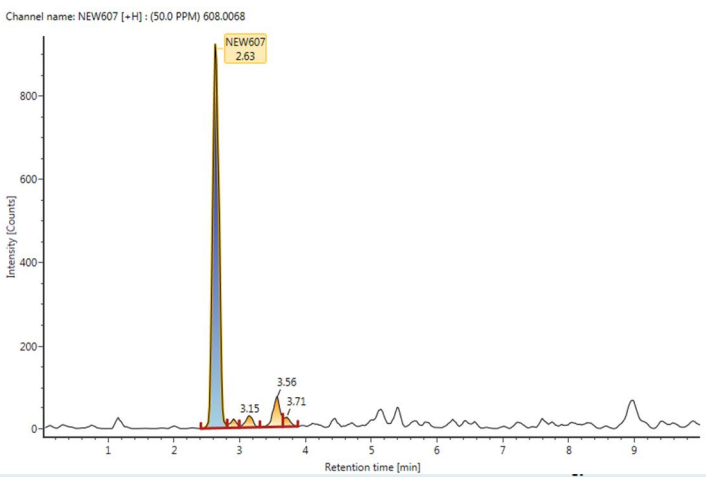

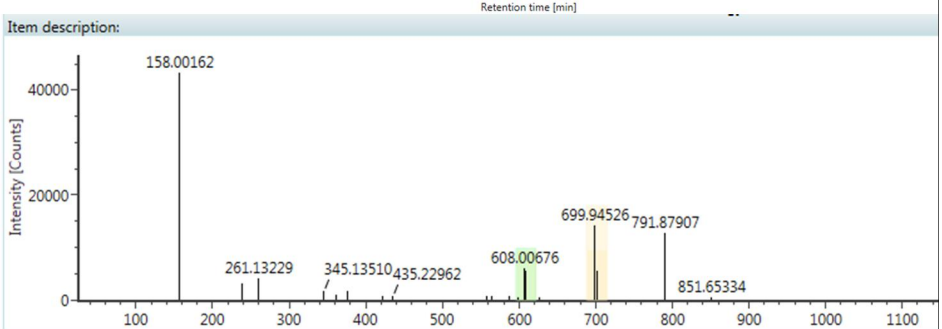

Byproduct
TP-606

Structure

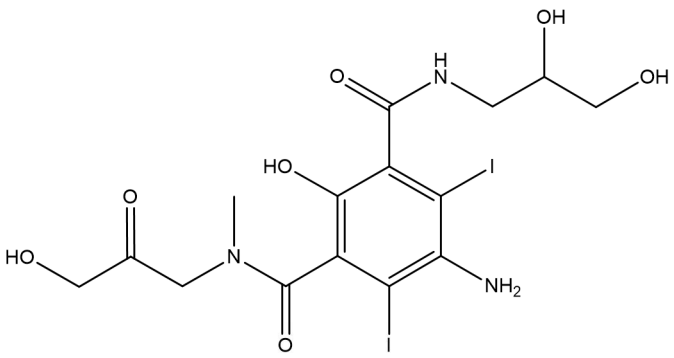

Chromatogram

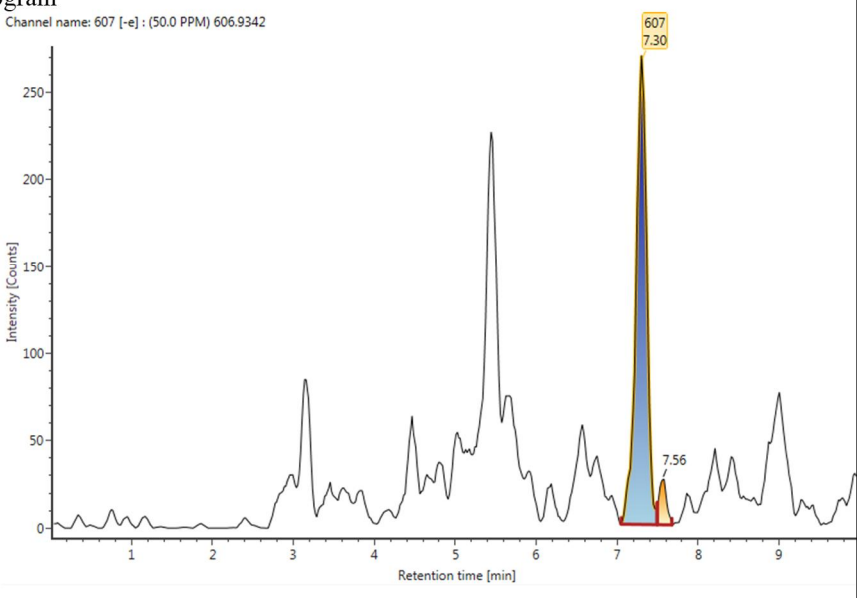

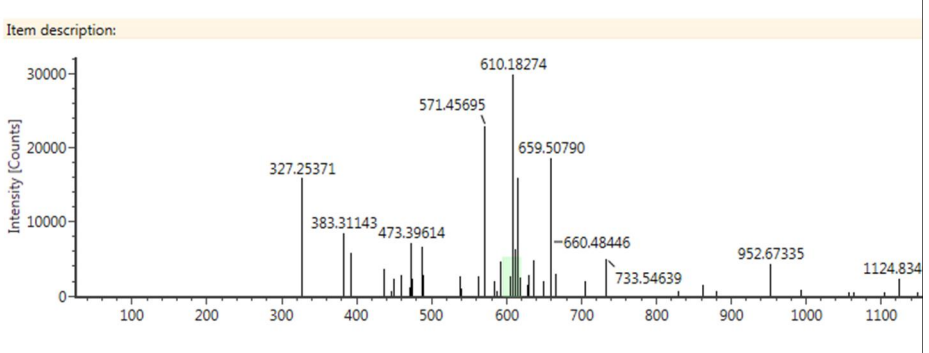

Table S7. Pseudo first-order rate constant of NB during UV-LED/chlorine process using 265 nm (1 $mWcm^{-2}$), 310 nm (41 $mWcm^{-2}$) and 365 nm (791 $mWcm^{-2}$) at different pH. $[IPM]_0$ = 10 μM, $[NB]_0$ = 10 μM, $[chlorine]_0$ = 10 mg/L, pH = 6, 7, 8, 9

	k'_{NB} **(Unit: sec^{-1})**		
	265 nm	**310 nm**	**365 nm**
pH 6	4.6×10^{-3}	1.1×10^{-2}	6.7×10^{-3}
pH 7	3.1×10^{-3}	8.3×10^{-3}	3.1×10^{-3}
pH 8	2.9×10^{-3}	7.1×10^{-3}	2.0×10^{-3}
pH 9	2.4×10^{-3}	6.8×10^{-3}	1.6×10^{-3}

Table S8. Pseudo first-order rate constant of NB during UV-LED/chlorine process using 265 nm (1 $mWcm^{-2}$), 310 nm (41 $mWcm^{-2}$) and 365 nm (791 $mWcm^{-2}$) at different pH. $[IPM]_0$ = 10 μM, $[NB]_0$ = 10 μM, $[chlorine]_0$ = 10 mg/L, pH = 6, 7, 8,

	k'_{NB} **(Unit: sec^{-1})**		
	265 nm	**310 nm**	**365 nm**
pH 6	5.87×10^{-3}	2.31×10^{-3}	1.97×10^{-5}
pH 7	3.1×10^{-3}	2.20×10^{-3}	1.71×10^{-5}
pH 8	2.9×10^{-3}	2.05×10^{-3}	1.39×10^{-5}
pH 9	2.4×10^{-3}	1.65×10^{-3}	1.00×10^{-5}

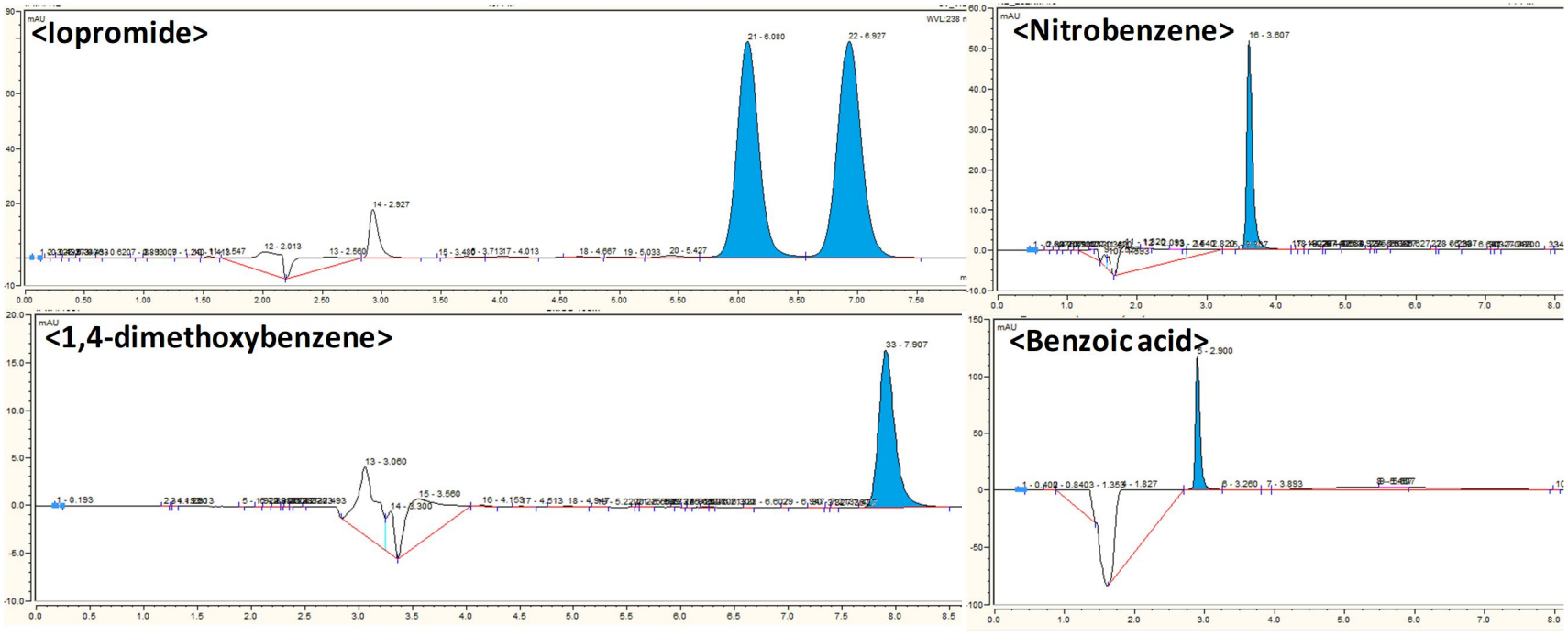

Fig. S1. Chromatograms of iopromide, nitrobenzene, benzoic acid, and 1,4-dimethoxybenzene and by HPLC.

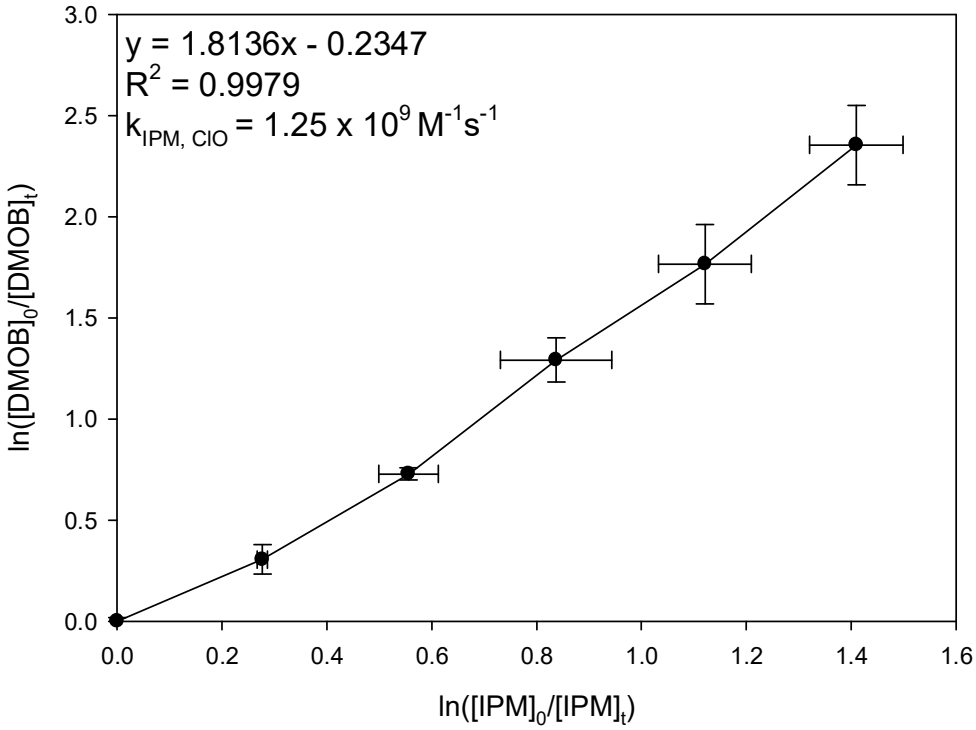

Fig. S2. Determination of second-order rate constant of ClO• reacting with IPM by the competition kinetics using DMOB during UV-LED/chlorine. (pH = 7, $[IPM]_0$ = 10 μM; $[DMOB]_0$ = 10 μM; [chlorine] = 10 mg/L, wavelength = 265 nm (1 mW cm^{-2})).

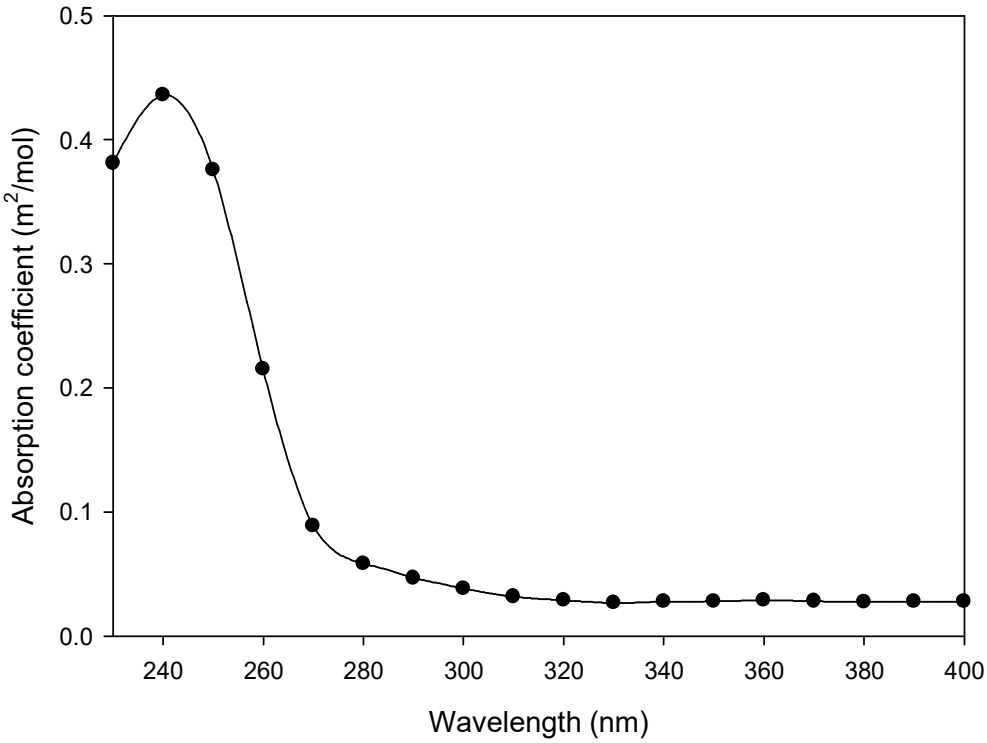

Fig. S3. UV absorption coefficient scan of IPM (pH = 5.8 (distilled water), [IPM] = 10 mg/L).

`